LOCALIZATION TECHNIQUES IN WIRELESS GEOPHONE NETWORKS FOR HIGH- DENSITY SEISMIC ACQUISITION

BY

Mansour Aljarbue

A Thesis Presented to the

DEANSHIP OF GRADUATE STUDIES

KING FAHD UNIVERSITY OF PETROLEUM & MINERALS

DHAHRAN, SAUDI ARABIA

In Partial Fulfillment of the
Requirements for the Degree of

MASTER OF SCIENCE

In

TELECOMMUNICATION ENGINEERING

April 2021

KING FAHD UNIVERSITY OF PETROLEUM & MINERALS

DHAHRAN- 31261, SAUDI ARABIA

DEANSHIP OF GRADUATE STUDIES

This thesis, written by Mansour Aljarbue under the direction of his thesis advisor and approved by his thesis committee, has been presented and accepted by the Dean of Graduate Studies, in partial fulfillment of the requirements for the degree of **MASTER OF SCIENCE IN TELECOMMUNICATION ENGINEERING.**

Dr. Suhail Ibrahim Al-Dharrab
(Advisor)

Dr. Abdallah S Al-Ahmari
Department Chairman

Dr. Samir Nasser Alghadhban
(Member)

Dr. Suliman Saleh Al-Homidan
Dean of Graduate Studies

3 May, 2021

Dr. Ali Arshad Nasir
(Member)

Date

Dedication

This theist is dictated to my mother Hessah and my brother Azzam and my Family

ACKNOWLEDGMENTS

Praise and glory to Allah, the Almighty with whose gracious mercy we live.

I would like to express my gratitude and profound appreciation to my advisor and thesis committee chairman, Dr. Suhail Ibrahim Al-Dharrab, for his guidance and support throughout the study. I could not have made it without his help; I wish Allah, the Almighty, reward him with all the best. I am also very grateful to my advisors and committee members, Dr. Samir Nasser Alghadhban and Dr. Ali Arshad Nasir, for their time and effort to review the thesis and provide valuable comments.

My special thanks go to my mother for her prayers and kindness, and also to my brother for encouraging me to pursue my Master degree. I thank them all for their support and for being next to me all the time. May Allah bless and reward them with all the good things in life.

TABLE OF CONTENTS

LIST OF TABLES

LIST OF FIGURES

LIST OF ABBREVIATIONS

WGN	Wireless Geophone Network
MLE	Maximum Likelihood Estimator
SDP	Semidefinite Programming
WLS	Weighted Least Square
LLS	Linear Least Square
DCC	Data Collection Center
GPS	Global Positioning System
RL	Receiver Line
SL	Source Line
IoT	Internet of Things
RSSI	Received Signal Strength Indicator
ROCRSSI	Ring Overlapping based on Comparison of Received Signal Strength Indicator
TOA	Time of Arrive
TDOA	Time Difference of Arrive
AOA	Angle of Arrive
NN	Neural Network
VA	Virtual Anchor
APIT	Approximate Point in Triangle
RMSE	Root-Mean-Square-Error
CRLB	Cramér-Rao Lower Bound
PEB	Position Error Bound
ULA	Uniform Linear Array
UWB	Ultra-Wide Band
AWGN	Additive White Gaussian Noise
GE	Genetic Algorithm
EP	Evolutionary Programming
DE	Differential Evolutionary
PSO	Particle Swarm Optimization

ABSTRACT

Full Name : [Mansour Aljarbue]
Thesis Title : [LOCALIZATION TECHNIQUES IN WIRELESS GEOPHONE NETWORKS FOR HIGH- DENSITY SEISMIC ACQUISITION]
Major Field : [MASTER OF SCIENCE IN TELECOMMUNICATION ENGINEERING]
Date of Degree : [April 2021]

Seismic data acquisition in oil and gas exploration is a challenging task due to the huge survey areas, e.g. up to 100 km^2, which requires thousands of geophones. Many companies rely on traditional cables to transfer the sensed/collected data from geophones to a Data Collection Center (DCC) using long cables, weights around 75% of the overall survey cost. Although cables are reliable for data transmission, their deployment, maintenance, and labor costs wireless data transfer an attractive alternative. Accurate positioning of geophones is crucial for the sensed data interpretation, which drives the need of power-efficient accurate positioning techniques for Wireless Geophones Networks (WGNs). This thesis will tackle this problem and propose novel approaches for energy-efficient WGN localization. We propose a realistic channel model for near-ground antennas, and cooperative localization techniques and compare it with non-cooperative localization techniques in WGNs. The proposed models showed that cooperative localization can enhance the localization performance greatly. For instance, at shadowing level of 4 dB standard deviation, we observed that cooperative localization can improve the accuracy by 80% compared to the noncooperative case and under the grid-deployment. Cooperative localization can be improved further by 41.1% using time of arrival techniques with additional complexity. Furthermore, the proposed channel parameters can affect the localization performance. Therefore, proper selection of the parameters can enhance the localization accuracy.

ملخص الرسالة

الاسم الكامل: **منصور الجربوع**

عنوان الرسالة: طرق تحديد مواقع مستشعرات الاهتزازات الأرضية اللاسلكية في عمليات التنقيب

التخصص: ماجستير العلوم في هندسة الاتصالات

تاريخ الدرجة العلمية: ابريل ٢٠٢١

يعد الحصول على البيانات الزلزالية للتنقيب عن النفط والغاز مهمة صعبة بسبب مساحة المسح الضخمة، على سبيل المثال تصل إلى 100 كيلومتر مربع، الأمر الذي يتطلب آلاف من مستشعرات الاهتزازات الأرضية. تعتمد العديد من الشركات في الوقت الحاضر على الكابلات التقليدية لنقل البيانات من مستشعرات الاهتزازات الأرضية إلى مركز جمع البيانات باستخدام الكابلات الطويلة، والتي تزن حوالي ٧٥٪ من التكلفة الإجمالية للمسح. على الرغم من أن الكابلات موثوقة لنقل البيانات، إلا أن نشرها وصيانتها واستكشاف الأعطال وإصلاحها والتكاليف اللوجستية والعمالة تجعل الخيارات الأخرى مثل نقل البيانات لاسلكيًا أكثر ملاءمة. ومع ذلك، فإن استبدال مستشعرات الاهتزازات الأرضية بمستشعرات لاسلكية يستلزم العديد من التحديات. أحد هذه التحديات هو سعة الطاقة المحدودة للمستشعرات اللاسلكية التي تعمل بالبطاريات، مما يحد القدرة على تزويد المستشعرات اللاسلكية بنظام تحديد المواقع العالمي. يعد تحديد المواقع بدقة للتنقيب أمرًا بالغ الأهمية لترجمة وتحليل البيانات المحسوسة والتي تم جمعها بشكل صحيح. لذلك، فإن هذا يدفع إلى الحاجة إلى تقنيات ذكية لتحديد مواقع المستشعرات بدقة عالية من خلال شبكات المستشعرات اللاسلكية. ستتطرق هذه الرسالة إلى هذه المشكلة وتقترح حلول مختلفة.

CHAPTER 1
INTRODUCTION

Land seismic acquisition is an essential part for oil and gas explorations and used for reflection seismology. This can be achieved by generating man-made vibrations (or seismic waves) on the earth's surface, varying their frequencies, and then sensing the reflected waves from earth's subsurface. Seismic data acquisition has three phases as shown in Figure 1. The first phase is the sweep phase, where the vibrating source generate elastic waves at the surface. After that, the listening phase where geophones listen to the reflected acoustic/elastic waves reflected from subsurface layers. Finally, the Move phase, where the seismic source, also known as the vibration point, proceeds to next survey spot. Vibration source can be either a vibrator truck or explosives [1].

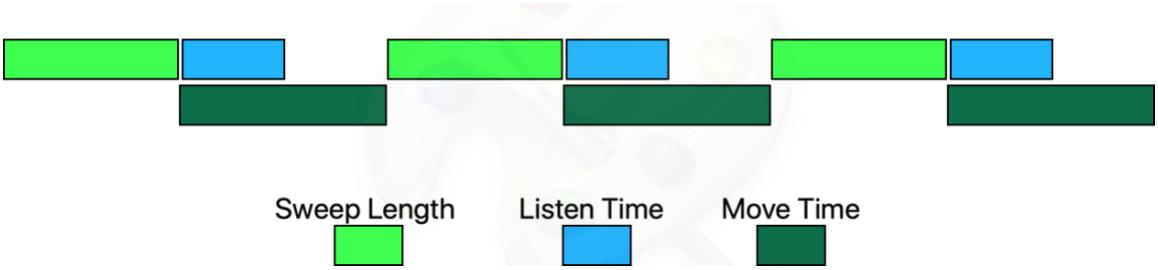

Figure 1: Seismic acquisition methodology [2]

Current geophones are connected through power and data cables to send sensed data to the Data Collection Center (DCC). Since the survey area is extremely large, it requires heavy and very long cables and equipment to cover the whole survey area [3]. Wired and cable-based connections provide a reliable and fast communication. However, their expensive

cost of deployment, maintenance, troubleshooting, manpower, and logistics make wireless data acquisition more favorable. In addition to the expensive cost, cable connection requires a significant time and effort for the full deployment and geophones' connections. Furthermore, the deployment of heavy batteries poses safety hazards for the crew in addition to possible damage to the ecosystem [3].

1.1 Land Seismic Acquisition

Land seismic acquisition in oil and gas explorations is conducted by generating vibrations on earth's surface of the survey area and distributing geophones at specific locations to sense the reflected waves from subsurface layers. In Figure 2, the concept is illustrated using a small-scale set up of seismic acquisition system with cable-based geophones. They report their sensed waves to the Seismograph, which analyze the data from all geophones. However, the survey areas in land seismic surveys might cover up to 100 Km^2 and require around 10,000-30,000 geophones. Geophones are typically deployed in the field in straight lines and typically spaced by 5-30 m [4]. These straight lines of geophones are called receiver lines (RLs). The vibrating source moves in straight lines perpendicular to RLs, which are called source lines (SLs) [1].

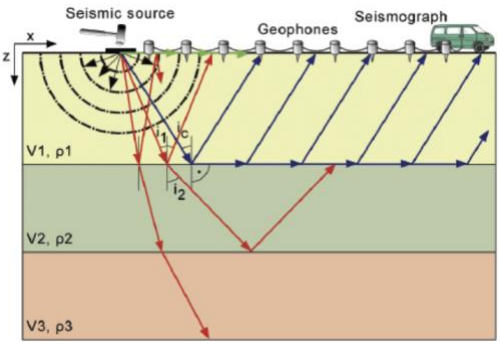

Figure 2:Small-scale seismic acquisition system using cable-based geophones [5]

1.2 Wireless Geophone Networks

Wireless geophone, shown in Figure 3, can be deployed in the oil and gas survey fields to sense the reflected acoustic waves generated by a vibrating source. Large number of wireless geophones will form a Wireless Geophone Network (WGN) that can sense the reflected seismic signals and transmit them to the DCC [6]. WGN consists mainly of wireless geophones, cluster-heads, and gateway nodes. The large-scale network is divided into clusters, and each cluster consists of wireless geophones and a cluster head. Wireless geophones are used only to sense and transmit data to cluster heads. Cluster heads then aggregate all data from nearby geophones and then send them to gateway nodes, which in turn forwards the collected data to the DCC [4].

Figure 3:SmartSolo wireless geophone (with 1.1 kg weight, 95mm X 103mm dimension and 38.48 Wh battery)

1.3 Geometrical System Layout

Large-scale high-density wireless geophones networks consist of more than 10,000 geophones to cover an area up to 100 km^2. Geophones are typically distributed in the survey area or field in parallel lines, known as a Receiver Lines (RLs), as shown in Figure 4. Geophones are placed approximately over equally spaced separations of 5-30 m. RLs are typically 200 m apart [1]. Gateways distribution is shown in Figure 4, where each cluster

forms a cell that covers several wireless geophones. Seismic sources, i.e. seismic vibrators mounted on trucks, move in orthogonal direction to RLs as depicted in Figure 4, which are known as source lines (SLs).

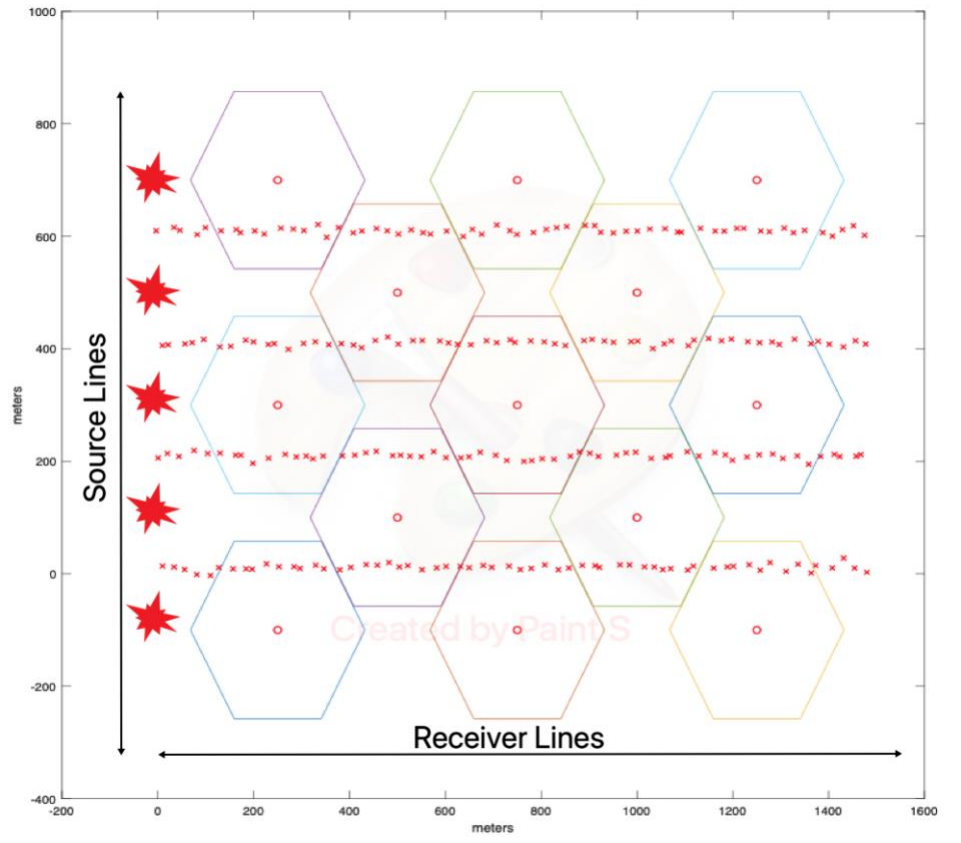

Figure 4: Orthogonal WGN deployment

Generally, self-localization in wireless sensor networks requires a minimum of three noncollinear anchors to localize a point in a 2-D space [7], [8]. Typically, geophones are deployed in a grid deployment (Figure 5) [1]. However, survey areas might prevent having the geophones in a grid-deployment due to the difficulty of placing geophones in some locations. Therefore, we will study the case where geophones are deployed in random deployment (Figure 6).

In our problem of wireless geophone localization, the scenarios of geophones geometry will be grid and random deployments. The performance of these scenarios will be examined and investigated in this thesis.

1.3.1 Grid-Based Deployment

WGNs typically have a grid-based deployment where thousands of geophones form Receiver Lines (RLs) to cover the survey area, as shown in Figure 4 [3]. Wireless geophones and gateways form clusters where a set of wireless geophones connected to nearby gateways as shown in Figure 4. Figure 5 shows a cluster in a grid-based deployment. The localization performance of grid-based deployment will be studied in this thesis. The same method can be carried on for the whole survey area, where geophones within the cluster can localize themselves with the aid of the nearby gateways that are equipped with GPS.

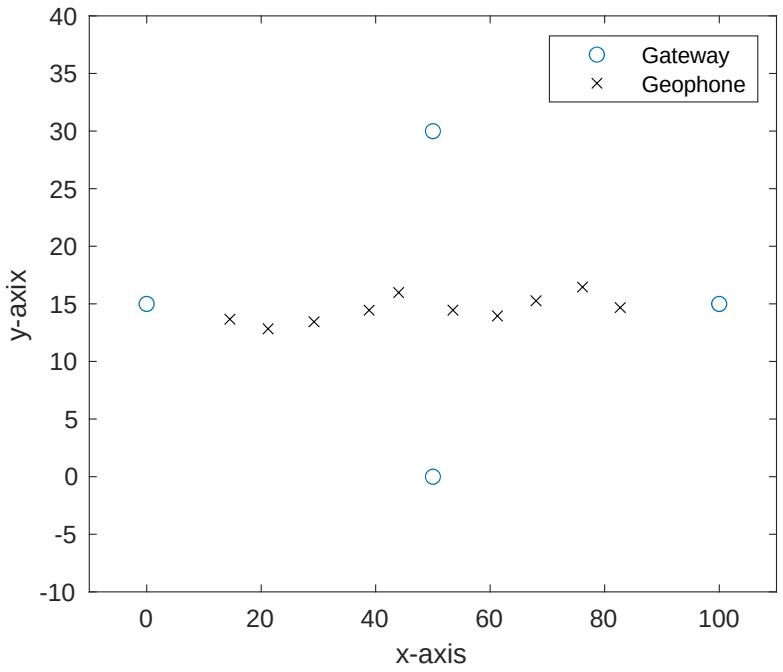

Figure 5: Grid Deployment of geophones

1.3.2 Random Deployment

It is occasionally encountered in seismic survey areas that partial segment of the survey area cannot have geophones placed in in grid-based fashion. This could be due to obstruction of reaching some locations in difficult terrains [9]. Therefore, this thesis will study the localization performance of geophones in random deployment as shown in Figure 6.

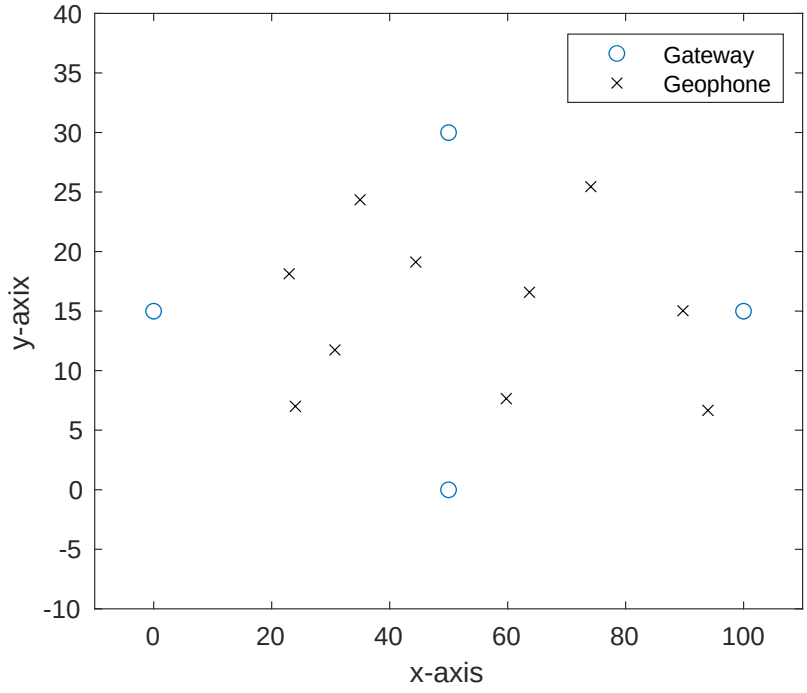

Figure 6: Random Deployment of geophones

1.4 Localization in Wireless Networks

Wireless Sensor Network (WSN) localization has been investigated intensively in recent years due to the trend of Internet of Things (IoT) and location-based services and the need for energy-efficient localization methods. For example, many wireless sensor nodes rely on the power-demanding Global Positioning System (GPS) antennas. Different localization

methods or algorithms are designed for the requirement in various applications. Localization can be done either pre-deployment, where nodes location is assigned manually, or post-deployment. Post-deployment localization can be categorized into node-self localization or target/source localization as shown in Figure 7 [10]. Node self-localization can be performed using triangulation, trilateration or the maximum likelihood method [10]. These methods rely on the different estimation techniques that estimate the distance between nodes. Furthermore, node self-localization can be either range-based or range-free localization.

Range-based localization is more accurate than Range-free localization since it measures the absolute distance between nodes [7]. Distance estimation in range-based localization can be based on Time of Arrival (TOA), Time Difference of Arrival (TDOA), Angle of Arrival (AOA) or Received Signal Strength Indication (RSSI) [7]. RSSI technique measures the signal strength and estimate the distance between nodes based on the path loss of transmitted signal. RSSI is the most power efficient localization method due its simplicity in term of hardware and processing power. However, it lacks the accuracy due to the error introduced by the additive noise and channel attenuation. TOA/TDOA estimates the distance based on the signal propagation period. They have better accuracy but require extra hardware and processing power [10]. AOA estimate the distance based on the angle of arrival. It requires antenna arrays, which is inefficient for low-cost sensors [10].

Range-free localization is less accurate than range-based localization since it does not measure the absolute distance between anchors nodes and the unknown node. In Hop-count-based range-free localization, distance is estimated by calculating the average hop

distance. This is computed by measuring the absolute distance between the anchors, equipped with GPS antennas, and then divide the Euclidean distance by number of hops between them. This results in the average of hop distance, which is used to locate the unknown node using triangulation, trilateration or the maximum likelihood method [10]. Pattern matching-based (Fingerprint) localization is commonly used as non-real time localization technique. It has two phases, where radio map is generated in the first phase. After that, the proximity is done by comparing the current radio signal to the radio map. Fingerprinting can lead to large localization error in crowded environments due to effects such as multipath, diffraction, and reflections. [7].

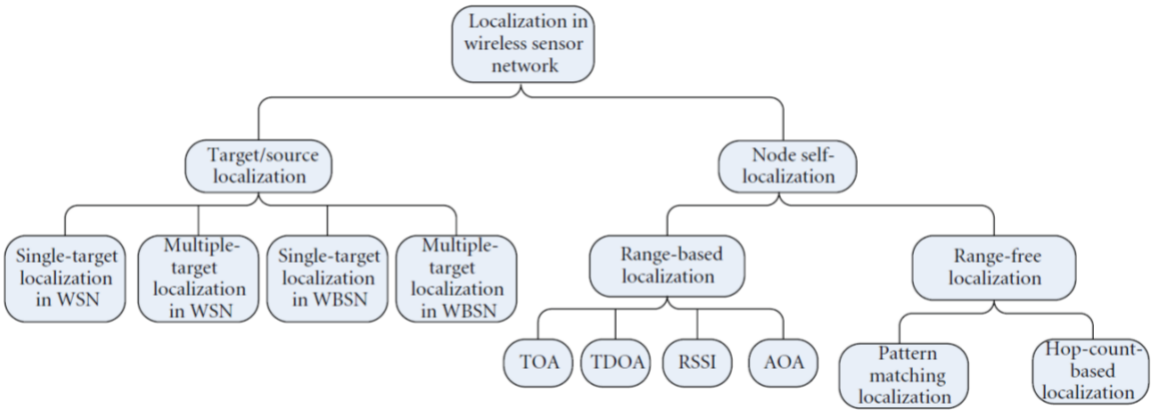

Figure 7: Localization methods [8]

1.5 Channel Models

Wireless propagation can follow different channel models depending on the propagation environment. Signal fading can be classified into large-scale and small-scale fading. Large-scale fading is the average signal attenuation due to moving over large distances and shadowing effects i.e. when obstacles between transmitter and receiver obstruct the signal. Small-scale fading is rapid changes of the signal over short time/distance caused by

multipath signal propagation or Doppler spread in the case of mobility. Log-Distance and Log-Normal-shadowing are the most well-known models that describe the large-scale fading, where the former one does not account for shadowing effect while the latter does. Small-scale fading in time-variant multipath channels can be described probabilistic models such as Rician and Rayleigh fading models. Rician and Rayleigh models are adopted in the case of large number of multipath components. Rician model is used in the multipath environment where Line-of-Sight (LOS) exists between transmitter and receiver, while Rayleigh is used in case of LOS does not exist between transmitter and receiver [11].

1.5.1 Log-Distance Propagation Model

Signal propagation model can vary differently depending on the propagation environment. Accurate pathloss model can be modeled by complex analytical expressions or empirical models that are applicable for only a short range of environments. However, there are generic pathloss models that can provide an acceptable propagation model with simple expression. Log-Distance pathloss model is one of the most famous pathloss models since it captures the essence of signal propagation in a simple model [11]. The Log-Distance propagation model is given by

$$PL_{Log-Distance} = 10\beta \log_{10} d \quad (1)$$

where β is the pathloss exponent and d is the Euclidean distance between transmitting and receiving antennas. The pathloss exponent changes depending on the propagation environment. Table 1 shows a list of different pathloss exponents, β, for different propagation environments.

Table 1: Pathloss Exponent for Different Environments [10]

Environment	$\boldsymbol{\beta}$
Urban macrocells	3.7-6.5
Urban microcells	2.7-3.5
Office Building (same floor)	1.6-3.5
Office Building (multiple floors)	2-6
Store	1.8-2.2
Factory	1.6-3.3
Home	3

Therefore, by manipulating the pathloss exponent, this pathloss model provide an insight about the signal propagation for large number of environments with simple expression.

1.5.2 Two-Ray Propagation Model

Two-Ray propagation model is used in an environment with one dominant multipath component, such as ground reflection. This thesis will examine flat-earth exploration terrain, where geophones' antennas are near to ground, and the ground reflection is significant [3]. The most suitable model in this scenario is the Two-Ray model, since the dominant multipath component is the ground reflection of the signal [12]–[15]. Rodríguez et al. in [13] investigated through measurements campaign the wireless access channels with near-ground level antennas for various outdoor scenarios. Based on their measurements, the propagation channel was well approximated by the Two-Ray path loss model. The path loss using the Two-Ray model is given by

$$PL_{(Two-Ray)} = 20\log\left(\left[\frac{\lambda}{4\pi}\right]\times\left|\frac{\sqrt{G_l}}{l}+\frac{R\sqrt{G_r}\,e^{-j\Delta\varphi}}{x+x'}\right|\right) \quad (2)$$

where λ is the carrier wavelength, G_l and G_r are the gains in the direction of LOS and ground reflection, respectively. G_l is defined as the product the of the antennas' gains (G_a and G_b) in LOS direction, while G_r is defined as the product of the antennas' gains (G_c and G_d) in the direction of ground reflection as shown in Figure 8. $\Delta\varphi$ denotes the phase

difference between LOS and ground reflected components. The reflection coefficient of the ground, R, is

$$R = \frac{\sin\theta - \sqrt{\varepsilon - \cos^2\theta}}{\sin\theta + \sqrt{\varepsilon - \cos^2\theta}} \tag{3}$$

which depends on the complex permittivity, ε, for the ground surface characteristics and the incident angle θ. The phase difference, and geometrical parameters, l, x, and x' (Figure 8) are defined by

$$\Delta\varphi = \frac{2\pi\,(x + x' - l)}{\lambda} \tag{4}$$

$$l = \sqrt{d^2 + (h_t - h_r)^2} \tag{5}$$

$$x + x' = \sqrt{d^2 + (h_t + h_r)^2} \tag{6}$$

where d is the Euclidean distance between transmitting and receiving antennas, h_t and h_r are the heights of transmitting and receiving antennas, respectively. The received signal strength is given by

$$P = P_0 - 20\log\left(\left[\frac{\lambda}{4\pi}\right] \times \left|\frac{\sqrt{G_l}}{l} + \frac{R\sqrt{G_r}\,e^{-j\Delta\varphi}}{x + x'}\right|\right) + n \tag{7}$$

where P and P_0 are the power of transmitted and received signals respectively in dBm. The log-normal shadowing, n, follows the Gaussian distribution $n \sim N(\mu, \sigma^2)$ where μ is the mean and σ is the standard deviation.

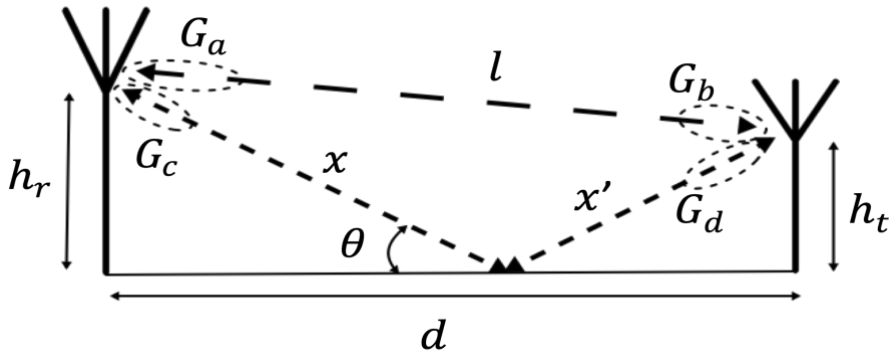

Figure 8: Two-Ray path loss model with respective parameters

1.5.3 Simplified Two-Ray Pathloss Model

Two-Ray pathloss model that has been discussed in previous section is excellent in term of precision of pathloss model when nodes and anchors are in a close proximity. When d is relatively large, $x + x' \approx l \approx d, \theta \approx 0$, $G_l \approx G_r$, and $R \approx -1$, then (7) can be simplified into the following pathloss model

$$P = P_0 + 10\log_{10}(G_r h_t^2 h_r^2) - 40\log_{10} d + n \tag{8}$$

The simplified Two-Ray pathloss model is a good approximation of the Two-Ray path loss model if the distance between the transmitter and receiver (d) exceeded the critical distance d_c as shown in Figure 9 [10]. d_c is given by

$$d_c = \frac{4h_t h_r}{\lambda} \tag{9}$$

Equation (8) can be written in an alternative way that can be useful in next sections

$$\Upsilon \times h = \alpha_0 \times 10^{\frac{n}{20}} \tag{10}$$

where $\Upsilon = 10^{\frac{P}{20}}$, $\alpha_{0j} = \sqrt{G_r} h_t h_r \, 10^{\frac{P_0}{20}}$, $h = d^2$. For sufficiently small noise $10^{\frac{n}{20}}$ can be approximated using first-order Tylor series expansion as $1 + \frac{\ln 10}{20} n$. Therefore, (10) can be approximated to

$$\Upsilon \times h = \alpha_0 + \epsilon \tag{11}$$

$$\epsilon = \frac{\alpha_0 \ln 10}{20} n \tag{12}$$

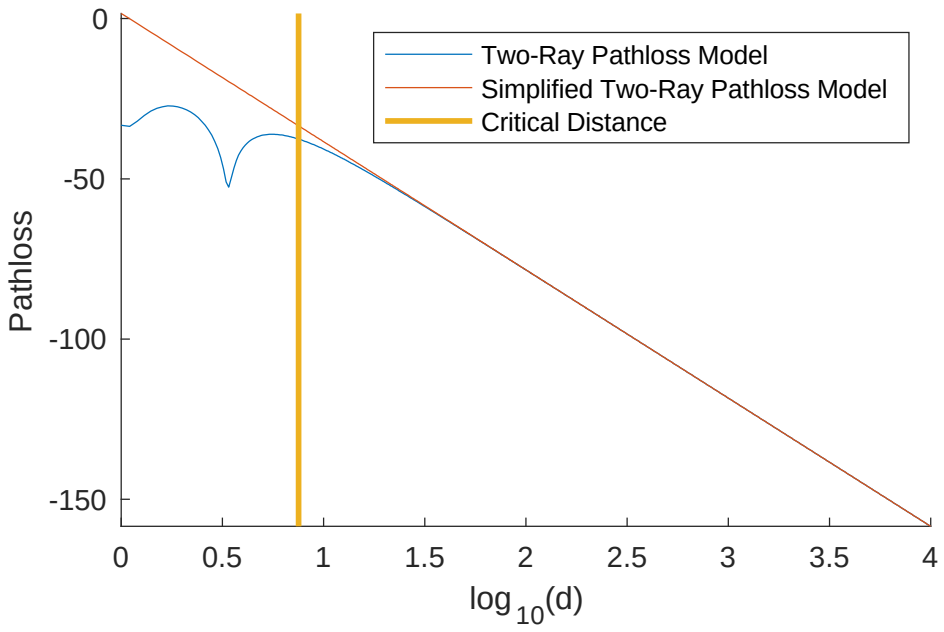

Figure 9: Two-Ray path loss model vs simplified Two-Ray path loss model

1.5.4 Localization Complexity in Ground Reflection Model

The pathloss model plays an essential role in the localization in term of accuracy and computational complexity. This thesis will examine the localization using Two-Ray pathloss model, which is more accurate in seismic survey environments due to the existence of the ground reflection multipath component. However, this model will impose a higher computational complexity. Figure 10 and Figure 11 show the 3-D localization objective functions of the Log-Distance and Two-Ray pathloss models respectively. It is clear that Two-Ray pathloss models is highly nonlinear and nonconvex compared to the Log-Distance pathloss model, which makes the localization complexity extremely higher.

This extreme complexity drives the need for simplified Two-Ray pathloss model, which is easier and faster to compute.

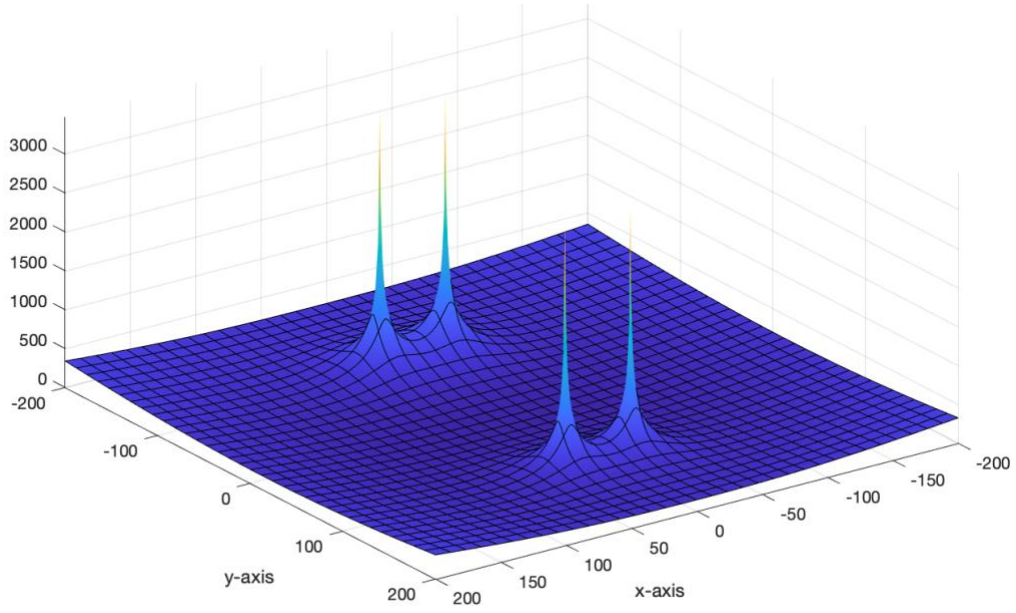

Figure 10: Localization objective function using log-distance pathloss model

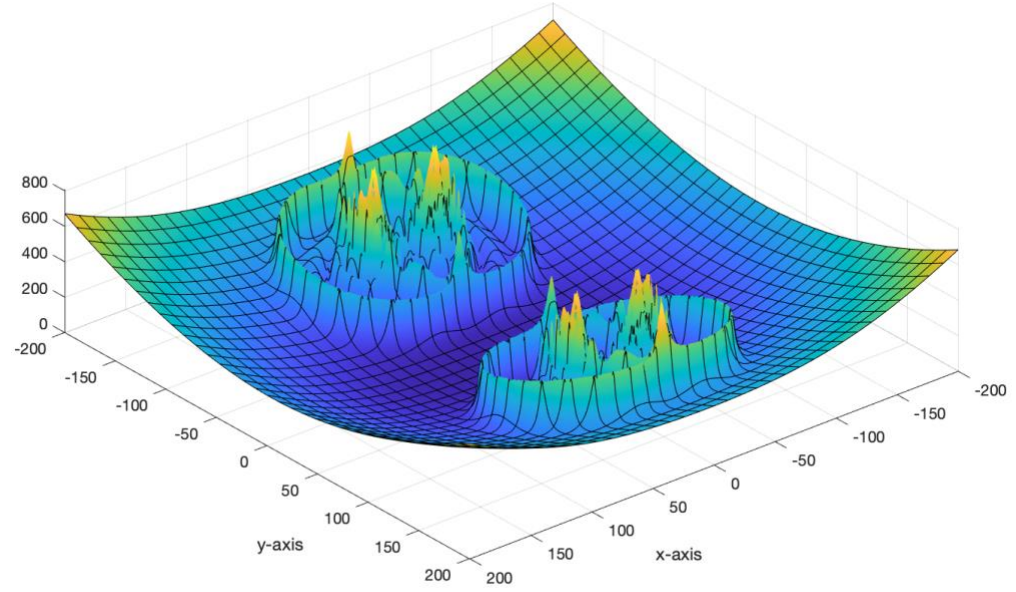

Figure 11: Localization objective function using Two-Ray pathloss model

1.6 Thesis Contributions

This thesis will examine and investigate the localization of WGN for high-density seismic acquisition. In the literature, RSSI based localization was mainly studied using Log-Distance pathloss model. In WGNs, this model might not be the ideal choice due multiple reasons. First, in seismic survey areas, signal propagation between transmitter and receiver can experience a severe constructive/destructive interference from the ground reflection. This is due to the fact that geophones normally have low-height antenna. Therefore, the ground reflection plays a major role in the received signal strength. Second, the Log-Distance pathloss model does not account for the carrier frequency, which affects the interference caused by the ground reflection. Third, the antennas heights can impact the received signal strength between nodes in WGN. Therefore, this thesis will study the localization of wireless geophone network adopting the Two-Ray pathloss propagation model, which provides an accurate signal propagation model for seismic survey areas. Furthermore, unlike most of the localization techniques, the proposed RSSI localization methods do not rely on the knowledge of the transmitted power from other nodes. We further derive mathematical lower bound expressions on the localization performance for the proposed estimation techniques and corroborate them with numerical simulations. Several parameters such as number of cooperating nodes, connectivity, antenna heights and gains, etc. were investigated and their effect on the localization accuracy. To the best of our knowledge, Two-Ray propagation model in a grid-based deployment of WGNs has not been investigated in RSSI localization. In addition to the noncooperative and cooperative localization using RSSI, this thesis will investigate and compare the TOA localization techniques and their associated complexities.

1.7 Thesis Outline

This thesis will be structured as follows. In Chapter 2, the literature review of different localization method will be reviewed and discussed. Specifically, the literature review on cooperative localization using RSSI and TOA localization techniques will be discussed. In Chapter 3, noncooperative localization will be introduced and investigated for seismic surveys. In Chapter 4, cooperative localization will be proposed for the wireless geophone network in both grid- and random-based deployments. In Chapter 5, TOA localization methods will be discussed and analyzed. Finally, the conclusions and future work are in Chapter 6.

CHAPTER 2

LITERATURE REVIEW

In this chapter, the literature review on wireless sensor network localization in general will be discussed. Then, we will present the cooperative localization and its various schemes in literature. We will then specifically focus the attention on two broad categories, namely, Received Signal Strength Indication (RSSI) and Time of Arrival (TOA) based localization techniques.

2.1 Localization Techniques in Wireless Sensor Network

WSN localization has attracted attention over the last few years, primarily for indoor applications. This can be rooted to the fast pace of IoT and WSN development for domains such as agriculture, military, and industrial applications, etc. GPS in certain cases is not a feasible positioning option due to its high-power consumption, expensive cost, and the need for line-of-sight (LOS) with satellites for accurate positioning [16]. Therefore, different energy-efficient localizations techniques have been investigated over the last decade. The most common localization techniques use range-based distance estimation in localization, which can be classified into Time of Arrival (TOA), Time Difference of Arrival (TDOA), Angle of Arrival (AOA) and RSSI [7], [17].

Cheng et al. in [10] provided a comprehensive review on WSN localization methodologies including source/target or node-self localizations. They also discussed distance estimation techniques, considering both range-based and range-free. Furthermore, they discussed

localization in case of non-line-of-sight (NLOS) and cooperative localization. They proposed to optimize the performance and energy consumption using localization scheduling mechanisms. Finally, they investigated the performance criteria such as average error or Root-Mean-Square-Error (RMSE) evaluation. There are advantages and disadvantages of adopting those localization techniques depending on the application. Azmi et al. in [18] reviewed various WSN localization techniques and compared different RSSI-based localization algorithms such as Min-Max, Multilateration, Maximum Likelihood, and Ring Overlapping based on Comparison of Received Signal Strength Indicator (ROCRSSI). They also described TDOA localization algorithms such as approximate maximum likelihood, two-stage maximum likelihood, and the use of genetic algorithms.

There have been several works in the literature on range-based localization techniques. R. Gong et al. in [19] introduced Multilateration localization methodology. RSSI ranging techniques was used for distance estimation. Then, they evaluated the localization performance experimentally. Laaouafy et al. in [20] introduced two localization methodologies, which are Trilateration and centroid. Trilateration is range-based localization while centroid is range-free localization. The performance is then evaluated using Cooja simulator. Khan et al. in [21] provided a comprehensive overview about different range-free localization. This includes Centroid, APIT (Approximate Point in Triangle), DV-Hop scheme, Multi-Hop and their subcategories.

Recently, there has been an increasing attention on the applications of wireless sensor networks. For example, oil and gas explorations rely on conducting land seismic surveys with thousands of geophones. S. Savazzi et al. in [4] provided a comprehensive overview

of land seismic survey and Wireless Geophone Network (WGN). They showed current limitations of wireless sensor networks solutions for land seismic acquisition. They proposed Ultra-Wide Band (UBW) wireless communication to provide high-speed data rate and accurate positioning. They showed the performance for cooperative and non-cooperative localization using TOA. The performance is corroborated with analytical Cramér-Rao Lower Bound on localization as a benchmark.

V. A. Reddy et al. in [22] proposed a cooperative localization for linear WGN using AoA over mm-wave communication. Localization performance limit is derived in terms of Cramér-Rao Lower Bound and worst-case position error bound (PEB) for single-hop and dual-hop cooperation in linear topologies. The path loss model considered was free space path loss, and localization performance was evaluated for different number of antenna arrays and distances.

A. Almehdar et al. in [23] proposed a localization method for WGN that use Deep Learning for AoA estimation. In this work, geophones assumed to have a single antenna while cluster-heads equipped with Uniform Linear Array (ULA) antennas. The channel model adopted does not account multipath fading effects. A neural network (NN) was used for AoA estimation, and the localization performance was investigated by comparing the performance of different NN with different hidden-layers and different neurons per hidden-layer.

We propose the Two-Ray path loss propagation model with RSSI-based localization technique in our wireless geophone network as the suitable model for seismic surveys with flat-earth environment, such as deserts. In this thesis, we will also compare the accuracy

and performance with different localization methods and derive the analytical limits in terms of Cramér Rao Lower Bounds.

2.2 Cooperative Localization Techniques

Classical localization algorithms mentioned in section 2.1 can be used between a node with unknown location and anchors. The minimum number of anchors required for localization is three noncollinear anchors based on the trilateration and triangulation algorithms. The localization accuracy has a direct relation with the number of anchors contributing in the localization. A novel method to improve the accuracy with same number of anchors is the cooperative localization. Cooperative localization is the method of localization in which all nodes with unknown locations cooperate with each other in the localization process. Nodes in RSSI-based localization report the sensed signal-power from other nodes to the anchors. After that, anchors estimate the distances between them and consider these distances in the localization process. This method improves substantially the localization accuracy.

Bouhdid et al. in [24] proposed an energy-aware cooperative localization method through RSSI ranging for trilateration. They proposed cooperative localization through three phases. First, a set of unknown nodes use classical localization method for localization by comparing the transmitted signal with the received signal and evaluate the distance. Next, these nodes broadcast themselves as virtual anchors (VA) for new sets of unknown nodes. The new sets will localize themselves based on the anchors and VAs. Theses anchors will only be considered if they exceed the confidence level threshold, which controls the accuracy of the localization.

Balaji et al. in [25] introduced cooperative trilateration technique for object localization. They introduced range-based and range-free localization. Then, they discussed the cooperative localization, where unknown nodes localize themselves, and then they broadcast their location. Other nodes with no nearby anchors can rely on these nodes for localization. Finally, they compared the localization accuracy of classical and cooperative localization.

Tomic et al. in [26] proposed a novel method that combines the RSSI and AOA ranging for 3-D nodes localization using Maximum likelihood estimator (MLE). The localization method described in [26] does not requires the knowledge of the transmitted power of sensors. Vaghefi et al. in [27], [28] proposed an RSSI localization method with unknown transmitted power. MLE estimator was used for localization. Furthermore, SDP relaxation was performed on the objective function and its localization performance is compared with MLE.

2.3 RSSI and TOA Based Techniques in Localization

RSSI and TOA are widely used ranging techniques for localization. RSSI is simpler in term of hardware and processing power compared to TOA. However, it lacks the accuracy due to the noise and shadowing effects on RSSI unlike TOA.

Researchers proposed different techniques that can enhance localizations accuracy in an energy-efficient manner. Zou et al. in [29] proposed a low complexity TOA localization algorithm that used iterative algorithm for MLE. They showed that the proposed algorithm outperforms traditional methods, such as weighted least square (WLS) and Taylor Series Expansion, with lower complexity. M. Laaraiedh et al. in [16] proposed a hybrid

localization technique that combines the ranging of RSSI, TOA, TDOA in order to enhance the positioning accuracy. Maximum likelihood (ML) and weighted least squares (WLS) were used for localization. Finally, a performance was compared for hybrid localization with classical localization RSSI or TOA or TDOA.

Wu et al. in [30] introduced TOA localization with a survey on various contributions to TOA localization methods. Synchronization and NLOS are the main sources of error in this technique. They proposed a TOA localization method that account for the NLOS and synchronization errors unlike the ones presented in literature. Its performance was compared to residual weighting algorithm, Quadratic Programming, and TOA.

CHAPTER 3

Noncooperative Localization in Wireless Geophone Networks

In this chapter, we first discuss the system and channel model for the noncooperative localization, then introduce the proposed estimation techniques. The optimization problem is then defined adopting the Two-Ray propagation channel model followed by the derivation of CRLB expression. Finally, the Monte-Carlo simulation of the localization performance under various shadowing levels will be discussed.

3.1 Introduction

Noncooperative localization is the classical localization method where the geophone sends a beacon signal that is sensed by at least three noncolinear gateways. The beacon signal is used by the gateways for distance or range estimation [7]. The most well-known ranging techniques are RSSI, TOA, TDOA and AOA. Once the distance is estimated between the geophone and the gateways, the position of the geophone can be estimated [31].

There is a wide range of estimation techniques that can vary in computational complexity and positioning accuracy. Accurate estimators tend to have more computational complexity [32]. Weighted Least Square (WLS) is an estimator better known for its simplicity; yet it lacks the accuracy if measurements are highly noisy [33]. On the other hand, MLE is excellent in terms of accuracy and it is asymptotically efficient [34] with relatively higher complexity. In this chapter, the performance of noncooperative localization will be investigated using different estimation techniques.

3.2 System and Channel Model

In this section, the system and channel model for noncooperative localization using Two-Ray pathloss model will be discussed. Let i and j be the indices of i^{th} gateway and j^{th} geophone, where $i \in \mathrm{C}$ and $j \in \mathcal{L}$. C is the set of indices of gateways, i.e. $\mathrm{C}= \{1,2,\dots,M\}$; and $\mathcal{L}$ is the set of indices of geophones, i.e. $\mathcal{L} = \{1,2,\dots,N\}$. Furthermore, let A_j and B_j be the set of indices of gateways and geophones connected to j^{th} geophone, respectively, such that $\mathrm{A}_j \subseteq \mathrm{C}$ and $\mathrm{B}_j \subseteq \mathcal{L}$. Let $\boldsymbol{y} = [\boldsymbol{y}_1, \dots, \boldsymbol{y}_M]^T$, $\boldsymbol{x} = [\boldsymbol{x}_1, \dots, \boldsymbol{x}_N]^T$ be the set of the gateways and geophones 2-D coordinates, respectively, where $\boldsymbol{y}_i = [a_i, b_i]^T$ and $\boldsymbol{x}_j = [x_j, y_j]^T \in \mathbb{R}^2$. Let $\boldsymbol{p_0} = [P_{01}, P_{02}, \dots, P_{0N}]^T$ denotes geophones' transmitted power (in dBm). The received signal strength (in dBm) at i^{th} gateway from j^{th} geophone is given by

$$P_{ij} = P_{0j} + 20\log\left(\left[\frac{\lambda}{4\pi}\right] \times \left|\frac{\sqrt{G_l}}{l_{ij}} + \frac{R_{ij}\sqrt{G_r}\, e^{-j\Delta\varphi_{ij}}}{x_{ij} + x'_{ij}}\right|\right) + n \qquad i \in \mathrm{A}_j \quad (13)$$

where n is the log-normal shadowing follows the Gaussian distribution $n \sim N(\mu, \sigma^2)$ and all other parameters are defined and discussed in detail in section 1.5.2. d_{ij} is the distance between i^{th} gateway and j^{th} geophone which is given by

$$d_{ij} = \sqrt{\left(x_j - a_i\right)^2 + \left(y_j - b_i\right)^2} \qquad i \in \mathrm{A}_j \quad (14)$$

As stated in section 1.5.3, if the distance between the nodes d_{ij} is asymptotically large, then $x_{ij} + x_{ij}{}' \approx l_{ij} \approx d_{ij}$, $\theta_{ij} \approx 0$, $G_l \approx G_r$, and $R_{ij} \approx -1$. Therefore, for $d = d_{ij}$, the expression in (8) can be rewritten as

$$P_{ij} = P_{0j} + 10\log_{10}(G_r h_t^2 h_r^2) - 40\log_{10}\left(d_{ij}\right) + n \qquad i \in \mathrm{A}_j \quad (15)$$

Furthermore, for $d = d_{ij}$, (11) and (12) can be written as

$$\Upsilon_{ij} \times h_{ij} = \alpha_{0j} + \epsilon_{0j} \qquad i \in \mathrm{A}_j \quad (16)$$

$$\epsilon_{0j} = \frac{\alpha_{0j}\ \ln 10}{20} n \tag{17}$$

where Υ_{ij} and h_{ij} are defined in subsection 1.5.3.

3.3 Proposed Estimation Techniques

We discuss in this section the proposed position estimation techniques in the wireless geophone networks under the Two-Ray propagation channel model.

3.3.1 Maximum Likelihood Estimation

Maximum Likelihood Estimation (MLE) is common method of parameter estimation due to its excellent performance, which approaches the CRLB asymptotically [34]. From (13) the MLE for the j^{th} geophone is defined as

$$\widehat{\boldsymbol{\vartheta}}_j = \underset{[\boldsymbol{x}_j, P_{0j}]\in\mathbb{R}^3}{\operatorname{argmin}} \sum_{i\in \mathrm{A}_j} \left[P_{ij} - P_{0j} + 20\log\left(\left[\frac{\lambda}{4\pi}\right] \times \left| \frac{\sqrt{G_l}}{l_{ij}} + \frac{R_{ij}\sqrt{G_r}\, e^{-j\Delta\varphi_{\mathrm{ij}}}}{x_{ij} + x'_{ij}} \right| \right) \right]^2 \tag{18}$$

where $\boldsymbol{\vartheta}_j = [\boldsymbol{x}_j, P_{0j}]$.

3.3.2 Weighted Least Square

Weighted least square (WLS) is a simple regression method that can be used for location estimation. It is extremely fast and has a simple computation complexity [27]. However, it lacks the accuracy for relatively large noise [33]. From (16) the WLS localization for the j^{th} geophone is defined as

$$\Upsilon_{ij} \times h_{ij} = \alpha_{0j} + \epsilon_{0\mathrm{j}} \tag{19}$$

Expanding the left-hand side of (19) and rearranging gives

$$2\Upsilon_{ij}\boldsymbol{y}_i^T\boldsymbol{x}_j - \Upsilon_{ij}\boldsymbol{x}_j^T\boldsymbol{x}_j + \ \alpha_{0j} = \Upsilon_{ij}\boldsymbol{y}_i^T\boldsymbol{y}_i + \epsilon_{0\mathrm{j}} \tag{20}$$

Let $\boldsymbol{\theta}_j = [\boldsymbol{x}_j^T,\ \boldsymbol{x}_j^T\boldsymbol{x}_j,\ \alpha_{0j}]$, then (19) can be written as

$$\boldsymbol{G}_j\boldsymbol{\theta}_j = \boldsymbol{h}_j + \boldsymbol{\epsilon}_j \tag{21}$$

$$\boldsymbol{G}_j = \begin{bmatrix} \vdots & & \\ 2\Upsilon_{ij}\boldsymbol{y}_i^T & -\Upsilon_{ij} & 1 \\ \vdots & & \end{bmatrix}, \qquad \boldsymbol{h}_j = \begin{bmatrix} \vdots \\ \Upsilon_{ij}\boldsymbol{y}_i^T\boldsymbol{y}_i \\ \vdots \end{bmatrix}, \qquad \boldsymbol{\epsilon}_j = \begin{bmatrix} \vdots \\ \epsilon_{0j} \\ \vdots \end{bmatrix} \tag{22}$$

$$\widehat{\boldsymbol{\theta}}_j = \left(\boldsymbol{G}_j{}^T\boldsymbol{W}_j\boldsymbol{G}_j\right)^{-1}\boldsymbol{G}_j{}^T\boldsymbol{W}_j\boldsymbol{h}_j \tag{23}$$

where $\boldsymbol{W}_j = \left[\frac{\alpha_{0j}\ln 10\,\sigma}{20}\right]^{-2}\boldsymbol{I}_{|\mathrm{A}_j|}$. α_{0j} is unknown and it can be omitted since it is a constant multiplied by $\boldsymbol{W}_j$.

3.3.3 Semidefinite Programming

Semidefinite Programming (SDP) is one of the best estimators in term of complexity and accuracy [27], [35]. From (16) the SDP localization for the j^{th} geophone is defined as

$$\left[\hat{\boldsymbol{x}}_j, \hat{\alpha}_{0j}\right] = \underset{[\boldsymbol{x}_j,\alpha_{0j}]}{\operatorname{argmin}} \sum_{i\in \mathrm{A}_j} \left(\Upsilon_{ij} \times h_{ij} - \alpha_{0j}\right)^2 \tag{24}$$

where Υ_{ij}, h_{ij} are given in subsection 1.5.3 with the Euclidean distance d_{ij} defined in (14). Equation (24) is nonlinear and nonconvex, later, we can convert it into a convex problem by defining an auxiliary variable $z_j = \boldsymbol{x}_j^T\boldsymbol{x}_j$. The minimization problem can be relaxed to an SDP optimization problem as

$$\underset{[\boldsymbol{x}_j,z_j,h_{ij},\alpha_{0\mathrm{j}}]}{\text{minimize}} \sum_{i\in \mathrm{A}_j} \left(\Upsilon_{ij} \times h_{ij} - \alpha_{0\mathrm{j}}\right)^2$$

subject to

$$h_{ij} = \begin{bmatrix}\boldsymbol{y}_i \\ -1\end{bmatrix}^T \begin{bmatrix}\boldsymbol{I}_2 & \boldsymbol{x}_j \\ \boldsymbol{x}_j^T & z_j\end{bmatrix} \begin{bmatrix}\boldsymbol{y}_i \\ -1\end{bmatrix} \qquad i \in \mathrm{A}_j$$

$$\begin{bmatrix}\boldsymbol{I_2} & \boldsymbol{x}_j \\ \boldsymbol{x}_j^T & z_j\end{bmatrix} \succcurlyeq \boldsymbol{0_3} \tag{25}$$

Now, (25) is a convex problem. This can be solved by convex optimization techniques [51].

3.4 Optimization Problem

In the previous section, we defined multiple noncooperative localization estimators for wireless geophones networks. These estimators rely on the fact that the minimum of objective function will result in estimated location [28]. In our situation, MLE is highly nonlinear and nonconvex. Therefore, linear and convex optimization techniques will not be applicable [36]. Since, the MLE is highly nonlinear and nonconvex, global minimization will not be guaranteed. Therefore, the initial starting point plays an essential role. This what drives the need for a simplified Two-Ray model, which serves as a starting point for MLE estimator. Nonlinear nonconvex optimization is a challenging subject, and the optimization techniques are normally complex. Since the computational capabilities of geophones and gateways are limited, complex optimization techniques will not be ideal solutions. Heuristic optimization methods can be used for nonlinear nonconvex. They have less computational complexity [37]. There are different Heuristic optimization methods such as Genetic Algorithm (GE), Evolutionary Programming (EP), Differential Evolutionary (DE), Particle Swarm Optimization (PSO) and many other methods. They are iterative random search methods, which provide good results with less computational complexity [32]. DE optimization method will be used for MLE minimization. For SDP, we will use the CVX toolbox in MATLAB. Table 2 shows the algorithm time complexity of different algorithms [27], [36]. It can be shown that DE will be more suitable for MLE than Gauss-Newton Algorithm due to its simplicity.

Table 2: Algorithms Complexity

Optimization Method	Iterations	Complexity per Iteration
ML (Gauss-Newton Algorithm)	k	$O\left(N^3\left(M+\frac{N}{2}\right)^3\right)$
ML (DE Algorithm)	k	$O(N)$
SDP	$\sqrt{N}\log(1/\epsilon)$	$O\left(N^4\left(M+\frac{N}{2}\right)^4\right)$
LLS	1	$O\left(6N^3\left(M+\frac{N}{2}\right)^2\right)$

3.4.1 Differential Evolutionary Algorithm

DE algorithm was introduced by Rainer Storn and Kenneth Price between 1994 and 1996. This algorithm was first proposed to solve the Chebychev Polynomial fitting problem. Later, this algorithm was used to solve complicated optimization problems [36], [38]. This algorithm is characterized by its simplicity and robustness and fast convergence toward the optimum solution [36]. It is population-based iterative optimization method which require (NP) population of candidate solutions $[\boldsymbol{X}_1, \boldsymbol{X}_2, \ldots, \boldsymbol{X}_{NP}]$, each with a dimension of size, D, such that $\boldsymbol{X}_i = \left[x_1^i, x_2^i, \ldots, x_D^i\right]$. The problem dimension, D, is based on the number of variables to be estimated. DE optimization algorithm has six main steps:

1. Initialization

The initial step is the specification optimization parameters, which are

D: The problem dimension of the candidate solutions $\boldsymbol{X}_i = \left[x_1^i, x_2^i, \ldots, x_D^i\right]$

NP: The population size $[\boldsymbol{X}_1, \ldots, \boldsymbol{X}_{NP}]$

N: Maximum Number of Iterations

F: Mutation Factor

CF: Crossover Factor

Once the optimization parameters are set. The initial population can be found as follows

$$x_j^i = x_{j,min}^i + rand \times \left(x_{j,max}^i - x_{j,min}^i\right) \qquad i \in NP, j \in D$$

where $x_{j,min}$ and $x_{j,max}$ defines the minimum and maximum range of the parameter need to be estimated, $rand$ is a random number such that $rand \sim U(0,1)$.

2. Evaluation and finding best solution

Once all the candidate solutions in the population are evaluated, the best solution $\boldsymbol{X}_{best}$ is stored.

3. Mutation

The mutation process starts with generating a new population or off-springs, where new solutions can be created by combining or mutating current solutions. Therefore, for every candidate solution $\boldsymbol{X}_i$, a new mutation vector $\boldsymbol{V}_i = \left[v_1^i, v_2^i, \dots, v_D^i\right]$ can be found as

$$\boldsymbol{V}_i = \boldsymbol{X}_{best} + F(\boldsymbol{X}_{r1} - \boldsymbol{X}_{r2})$$

$\boldsymbol{X}_{r1}, \boldsymbol{X}_{r2}$ are random solutions from current population. The mutation Factor, F, plays an important role in the convergence speed.

4. Crossover

Crossover process can enhance the diversity of the search space and hence the optimization performance. In crossover operation, each the candidate solution $\boldsymbol{X}_i$ and the mutant vector $\boldsymbol{V}_i$ create a new trail vector $\boldsymbol{T}_i$. Let $\boldsymbol{T}_i = \left[t_1^i, t_2^i, \dots, t_D^i\right]$, therefore, $\boldsymbol{T}_i$ can be found as

$$t_j^i = \begin{cases} v_j^i, & rand < CR \\ x_j^i, & rand \geq CR \end{cases}$$

5. Selection

The selection process is the last step of the iteration, which provide a new population for the new iteration. The new population can be found by comparing the objective function

value of the candidate solution $\boldsymbol{X_i}$ and the mutated/cross-covered trail $\boldsymbol{T_i}$, then select the better one in term of objective function fitness.

6. Stopping criteria

The stopping criteria is a problem dependent. However, the number of iterations must not exceed the maximum number of iterations defined in the initialization step.

DE Algorithm

```
Specify control parameters (NP, D, F, CR, N)
Generate random population
x_i^i = x_{j,min}^i + rand × (x_{j,max}^i − x_{j,min}^i) i ∈ NP, j ∈ D
Find X_best
While termination condition is not satisfied
      for i = 1 to NP
            Generate two indices r1, r1 with r1 ≠ r2
            V_i = X_best + F(X_r1 − X_r2) % Mutation
            for j = 1 to D
                  if rand < CR
                  t_j^i = v_j^i % crossover
                  else
                  t_j^i = x_j^i % crossover
                  end % end if

                  if
                  f(T_i) < f(X_i) %Selection
                  X_i = T_i
                  else
                  Don't change X_i
                  end % end if
            end %end of D
      end %end of NP
      update X_best
end % end While
```

Figure 12: DE algorithm

3.5 Cramér Rao Lower Bound Derivation

Cramér-Rao Lower Bound (CRLB) is defined as the lower limit of the variance of any unbiased estimator [34]. In this section, the CRLB for RSSI localization with unknown transmitted power will be derived. Let $\boldsymbol{\psi}_j = [\boldsymbol{x}_j, P_{0j}]$, then the log Maximum-Likelihood (ML) function of (13) is defined as

$$\ln p(\boldsymbol{p}_j, \boldsymbol{\psi}_j) = k - \sigma^2 \left(\boldsymbol{\mu}(\boldsymbol{\psi}_j) - \boldsymbol{p}_j\right)^T \left(\boldsymbol{\mu}(\boldsymbol{\psi}_j) - \boldsymbol{p}_j\right) \tag{26}$$

where

$$\boldsymbol{\mu}\left(\boldsymbol{\psi}_j\right) = \begin{bmatrix} \cdot \\ \cdot \\ \mu_{ij} \\ \cdot \\ \cdot \end{bmatrix}_{i \in \mathrm{A}_j} \qquad \boldsymbol{p}_j = \begin{bmatrix} \cdot \\ \cdot \\ P_{ij} \\ \cdot \\ \cdot \end{bmatrix}_{i \in \mathrm{A}_j}$$

$$\mu_{ij} = P_{0j} + 20 \log\left(\left[\frac{\lambda}{4\pi}\right] \times \left|\frac{\sqrt{G_l}}{l_{ij}} + \frac{R_{ij}\sqrt{G_r}\, e^{-j\Delta\varphi_{ij}}}{x_{ij} + x'_{ij}}\right|\right)$$

Therefore, the CRLB for $\boldsymbol{\psi}_j$ is defined as

$$CRLB(\boldsymbol{\psi}_j) = diag\left(\mathrm{J}^{-1}(\boldsymbol{\psi}_j)\right) \tag{27}$$

where $\mathrm{J}(\boldsymbol{\psi}_j)$ is the Fisher information matrix which is given by

$$\mathrm{J}(\boldsymbol{\psi}_j) = \sigma^{-2} \left[\frac{\partial \ln p(\boldsymbol{p}_j, \boldsymbol{\psi}_j)}{\partial \boldsymbol{\psi}_j}\right]^T \left[\frac{\partial \ln p(\boldsymbol{p}_j, \boldsymbol{\psi}_j)}{\partial \boldsymbol{\psi}_j}\right] = \sigma^{-2} \boldsymbol{F}^T \boldsymbol{F} \tag{28}$$

where

$$\begin{gathered} \boldsymbol{F} = \frac{\partial \boldsymbol{\mu}(\boldsymbol{\psi}_j)}{\partial \boldsymbol{\psi}_j} = \begin{bmatrix} \boldsymbol{F}_1 \\ \cdot \\ \boldsymbol{F}_j \\ \cdot \\ \boldsymbol{F}_N \end{bmatrix}, \quad \boldsymbol{F}_j = \begin{bmatrix} \cdot \\ \cdot \\ \boldsymbol{f}_{ij} \\ \cdot \\ \cdot \end{bmatrix}_{i \in \mathrm{A}_j \cup \mathrm{B}_j} \\ \boldsymbol{f}_{ij} = \left[\frac{\partial \mu_{ij}}{\partial x_j}, \frac{\partial \mu_{ij}}{\partial y_j}, \frac{\partial \mu_{ij}}{\partial P_{0\mathrm{j}}}\right] \end{gathered} \tag{29}$$

$$\frac{\partial \mu_{ij}}{\partial x_j} = \frac{\partial \mu_{ij}}{\partial d_{ij}} * \frac{\partial d_{ij}}{\partial x_j}, \qquad \frac{\partial \mu_{ij}}{\partial y_j} = \frac{\partial \mu_{ij}}{\partial d_{ij}} * \frac{\partial d_{ij}}{\partial y_j}, \qquad \frac{\partial \mu_i}{\partial P_{0\mathrm{j}}} = 1$$

$$\frac{\partial \mu_{ij}}{\partial d_{ij}} = \frac{10}{\ln(10) \times \left(\left(\frac{\sqrt{G_l}}{l_{ij}} + \frac{\sqrt{G_r} R_{ij}}{x_{ij} + x'_{ij}} \cos \Delta\varphi_{ij} \right)^2 + \left(\frac{\sqrt{G_r} R_{ij}}{x_{ij} + x'_{ij}} \sin \Delta\varphi_{ij} \right)^2 \right)}$$

$$\times \left(\left[2 \times \left(\frac{\sqrt{G_l}}{l_{ij}} + \frac{\sqrt{G_r} R_{ij}}{x_{ij} + x'_{ij}} \cos \Delta\varphi_{ij} \right) \right.\right.$$

$$\times \left(\sqrt{G_l} \left(\frac{-d_{ij}}{{l_{ij}}^3} \right) \right.$$

$$\left.\left. + \sqrt{G_r} \left(\frac{-d_{ij}}{\left[x_{ij} + x'_{ij} \right]^3} \right) \cos \Delta\varphi_{\mathrm{ij}} \times \frac{-\sin \Delta\varphi_{ij}}{x_{ij} + x'_{ij}} \right.\right.$$

$$\left.\left. \times \left(\frac{2\pi}{\lambda} \left(\frac{d_{ij}}{\left(x_{ij} + x'_{ij} \right)} - \frac{d_{ij}}{l_{ij}} \right) \right) \right) \right] \qquad (30)$$

$$+ \left[2 \times \left(\frac{\sqrt{G_r} R_{ij}}{x_{ij} + x'_{ij}} \sin \Delta\varphi_{ij} \right) \right.$$

$$\times \left(\sqrt{G_r} \left(\frac{-d_{ij}}{\left[x_{ij} + x'_{ij} \right]^3} \right) \sin\ \Delta\varphi_{ij} \times \frac{\cos \Delta\varphi_{ij}}{x_{ij} + x'_{ij}} \right.$$

$$\left.\left. \times \left(\frac{2\pi}{\lambda} \left(\frac{d_{ij}}{\left(x_{ij} + x'_{ij} \right)} - \frac{d_{ij}}{l_{ij}} \right) \right) \right) \right] \right)$$

$$\frac{\partial d_{ij}}{\partial x_j} = \frac{-\left(a_i - x_j \right)}{d_{ij}} \qquad i \in \mathrm{A}_j \qquad (31)$$

$$\frac{\partial d_{ij}}{\partial y_i} = \frac{-\left(b_i - y_j \right)}{d_{ij}} \qquad i \in \mathrm{A}_j \qquad (32)$$

3.6 Numerical Results and Discussion

In this section, we will discuss the performance of the proposed estimators for noncooperative localizations in the cases of grid-based deployment and random-based deployment depicted in Figure 5 and Figure 6, respectively. The estimators that are used for noncooperative localization are: WLS, MLE and SDP. SDP estimator in (25) is a convex optimization technique that converge to the global minima without initialization step. Furthermore, WLS estimator in (23) is a linear estimator that does not require initialization step. However, MLE estimator in (18) is nonlinear and nonconvex. Therefore, initialization is needed, and it plays a major role. We used SDP estimation as a starting point of MLE estimator. MLE uses DE optimization algorithm as shown in Figure 12. Monte-Carlo simulations have been performed to see the performance of the estimators for grid-based and random-based deployments. These estimators are benched-marked with CRLB which is the minimum variance on any unbiased estimator. Table 3 lists the simulation parameters used in the numerical simulation for the localization accuracy.

Table 3: Simulation Parameters of Noncooperative Localization

Simulation Parameter	**Value**
Average transmit power	10 dBm
h_t	0.8 m
h_r	1.5 m
f	470 MHz
G_l	1
G_r	1
ε	3.0000 - 0.0038i

Figure 13 and Figure 14 show the Root-Mean-Square-Error (RMSE) versus the shadowing standard deviation (σ). The RMSE is calculated based on 500 noise realizations. From the simulations, we can clearly see that the standard deviation of the shadowing affects WLS

estimator heavily. On the other hand, SDP estimator performance is much better, and it is close to MLE initialized with the correct solution. Furthermore, we can see that the deployment of geophones has an impact on the localization error. For WLS, the grid deployment localization error is lower than the error in random deployment. However, for MLE and SDP estimators the performances of both deployments are comparable.

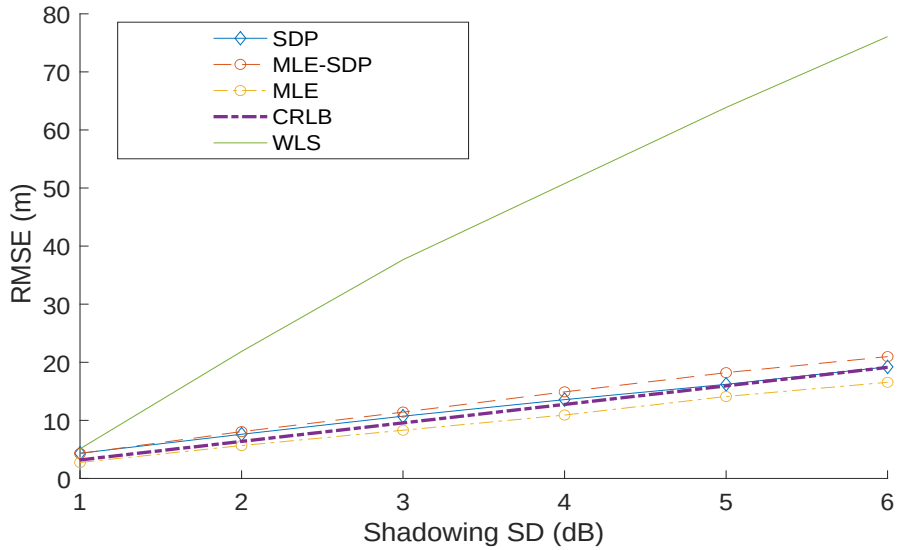

Figure 13: Noncooperative localization performance for different estimators (Random-based Deployment)

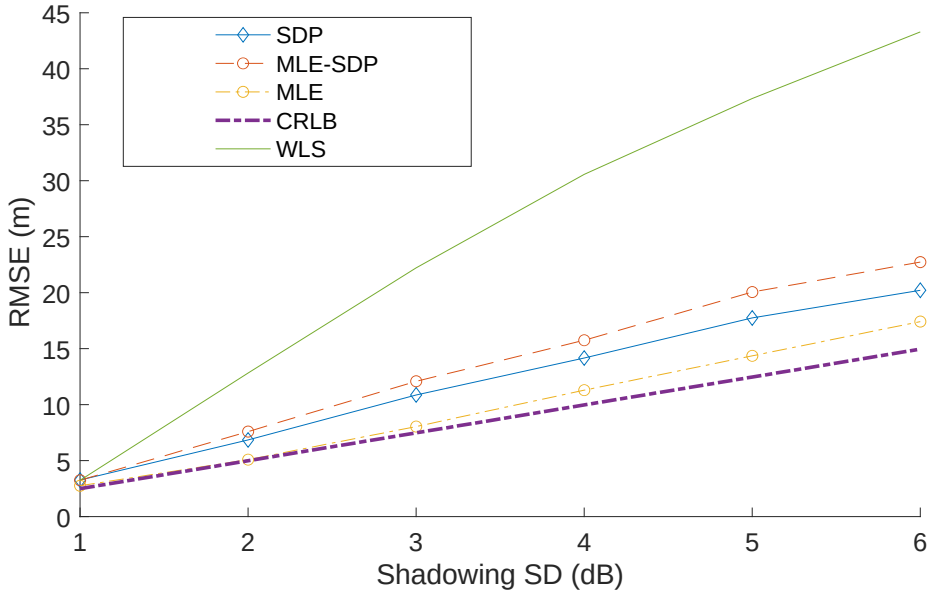

Figure 14: Noncooperative localization performance for different estimators (Grid-Based Deployment)

CHAPTER 4

Cooperative Localization in Wireless Geophone Network

In this chapter, we first introduce the system and channel model for the cooperative localization and associated position estimation techniques. The optimization problem is stated using the Two-Ray propagation channel model and the CRLB expression is then derived. The extensive numerical simulations of the localization performance under various shadowing levels will be performed considering effect of number of cooperative nodes, connectivity, antenna heights and gains will be investigated.

4.1 Introduction

Cooperative localization is a novel method of engaging and exploiting geophones as gateways for localization. In cooperative localization, each geophone sends a beacon signal that can be heard by nearby gateways and geophones [39], [40]. Nearby geophones will report the sensed signals to nearby gateways. Gateways, which are equipped with GPS, will utilize the sensed signals from both gateways and geophones to estimate the geophones' locations [39]. Cooperative localization can impose more computational complexity. However, it can increase the localization accuracy greatly since the number of measurements will be increase and hence the accuracy will increase [41].

All ranging techniques that have been discussed in Chapter 3 are applicable for cooperative localization. Furthermore, the estimation and optimization techniques that are applicable for cooperative localization, which will be investigated in the subsequent sections.

4.2 System and Channel Model

The system and channel model for cooperative localization will be an extension to the noncooperative model discussed in section 3.2. Let A_j and B_j be the set of gateways and geophones connected to j^{th} geophone respectively, such that $A_j \subseteq \mathbb{C}$ and $B_j \subseteq \mathcal{L}$. Let $\boldsymbol{y} = [\boldsymbol{y}_1, \dots, \boldsymbol{y}_M]^T$, $\boldsymbol{x} = [\boldsymbol{x}_1, \dots, \boldsymbol{x}_N]^T$ be the set of the gateways and geophones 2-D coordinates respectively where $\boldsymbol{y}_i = [a_i, b_i]^T$ and $\boldsymbol{x}_j = [x_j, y_j]^T \in \mathbb{R}^2$. Let $\boldsymbol{p_0} = [P_{01}, P_{0j}, \dots, P_{0N}]^T$ denote geophones' transmitted power (in dBm) respectively. The received signal strength (in dBm) at i^{th} gateway from j^{th} geophone is given by

$$P_{ij} = P_{0j} + 20\log\left(\left[\frac{\lambda}{4\pi}\right] \times \left|\frac{\sqrt{G_l}}{l_{ij}} + \frac{R_{ij}\sqrt{G_r}\, e^{-j\Delta\varphi_{ij}}}{x_{ij} + x'_{ij}}\right|\right) + n \qquad i \in A_j \cup B_j \qquad (33)$$

This model and all its parameters are discussed in detail in section 1.5.2. d_{ij} is defined as the distance between i^{th} gateway (or geophone) and j^{th} geophone which is given by

$$\begin{aligned} d_{ij} &= \sqrt{(x_j - a_i)^2 + (y_j - b_i)^2} && i \in A_j \\ d^c_{ij} &= \sqrt{(x_j - y_i)^2 + (y_j - y_i)^2} && i \in B_j \end{aligned} \qquad (34)$$

where d^c_{ij} denotes the distance between collaborating nodes. As stated in section 1.5.3, if the distance between the nodes d_{ij} is asymptotically large, then $x_{ij} + x_{ij}' \approx l_{ij} \approx d_{ij}$, $\theta_{ij} \approx 0$, $G_l \approx G_r$, and $R_{ij} \approx -1$. Therefore, for $d = d_{ij}$, expression in (8) can be written as

$$P_{ij} = P_{0j} + 10\log_{10}(G_r h_t^2 h_r^2) - 40\log_{10}(d_{ij}) + n \qquad i \in A_j \cup B_j \qquad (35)$$

Furthermore, for $d = d_{ij}$ (11) and (12) can be written as

$$\Upsilon_{ij} \times h_{ij} = \alpha_{0j} + \epsilon_{0j} \qquad i \in A_j \cup B_j \qquad (36)$$

$$\epsilon_{0j} = \frac{\alpha_{0j} \ln 10}{20} n \qquad i \in \mathrm{A}_j \cup \mathrm{B}_j \qquad (37)$$

4.3 Proposed Estimation Techniques

In this section, we introduce the proposed cooperative position estimation techniques in the wireless geophone network under the Two-Ray propagation model.

4.3.1 Maximum Likelihood Estimation

Maximum Likelihood Estimation (MLE) for cooperative localization will be an extension of (18) where measurements between geophones are utilized to enhance the location estimation. Therefore, MLE for cooperative localization is defined as

$$\widehat{\boldsymbol{\Psi}} = \underset{[\boldsymbol{x},\boldsymbol{p}]\in\mathbb{R}^{3\mathrm{N}}}{\operatorname{argmin}} \sum_{j\in\mathcal{L}} \sum_{i\in \mathrm{A}_j \cup \mathrm{B}_j} \left[P_{ij} - P_{0j} + 20 \log\left(\left[\frac{\lambda}{4\pi}\right] \times \left| \frac{\sqrt{G_l}}{l_{ij}} + \frac{R_{ij}\sqrt{G_r}\, e^{-j\Delta\varphi_{ij}}}{x_{ij} + x'_{ij}} \right| \right) \right]^2 \qquad (38)$$

where $\boldsymbol{\Psi} = [\boldsymbol{x}, \boldsymbol{p}_0]$.

4.3.2 Semidefinite Programming

Semidefinite Programming (SDP) for cooperative localization is an extension of (25). The auxiliary variable will be extended to be $\boldsymbol{z} = \boldsymbol{x}^T\boldsymbol{x}$. Therefore, cooperative SDP is defined as

$$\underset{[\boldsymbol{x},\boldsymbol{z},h_{ij},\alpha_{0\mathrm{j}}]}{\text{minimize}} \sum_{j\in\mathcal{L}} \sum_{i\in \mathrm{A}_j \cup \mathrm{B}_j} \left(\Upsilon_{ij} \times h_{ij} - \alpha_{0\mathrm{j}}\right)^2$$

subject to

$$h_{ij} = \begin{bmatrix} \boldsymbol{y}_i \\ -\mathbf{e}_j \end{bmatrix}^T \begin{bmatrix} \boldsymbol{I}_2 & \boldsymbol{x} \\ \boldsymbol{x}^T & \boldsymbol{z} \end{bmatrix} \begin{bmatrix} \boldsymbol{y}_i \\ -\mathbf{e}_j \end{bmatrix} \qquad i \in \mathrm{A}_j$$

$$h_{ij} = \begin{bmatrix} \mathbf{0}_2 \\ \mathbf{e}_i - \mathbf{e}_j \end{bmatrix}^T \begin{bmatrix} \boldsymbol{I}_2 & \boldsymbol{x} \\ \boldsymbol{x}^T & \boldsymbol{z} \end{bmatrix} \begin{bmatrix} \mathbf{0}_2 \\ \mathbf{e}_i - \mathbf{e}_j \end{bmatrix} \qquad i \in \mathrm{B}_j$$

$$\begin{bmatrix} \boldsymbol{I}_2 & \boldsymbol{x} \\ \boldsymbol{x}^T & \boldsymbol{z} \end{bmatrix} \succcurlyeq \boldsymbol{0}_{N+2} \tag{39}$$

4.4 Optimization Problem

The optimization techniques for cooperative localization are similar to noncooperative localization. DE optimization method will be used for MLE. MATLAB CVX toolbox will be used for SDP.

4.5 Cramér Rao Lower Bound Derivation

Cramér-Rao Lower Bound (CRLB) is defined the lower limit of the variance of any unbiased estimator. In this section, the CRLB for RSSI localization with unknown transmitted power will be derived for cooperative localization. Let $\boldsymbol{\psi} = [\boldsymbol{x}, \boldsymbol{p_0}]$, then the log ML function is defined as

$$\ln p(\boldsymbol{p}, \boldsymbol{\psi}) = k - \sigma^2 (\boldsymbol{\mu}(\boldsymbol{\psi}) - \boldsymbol{p})^T (\boldsymbol{\mu}(\boldsymbol{\psi}) - \boldsymbol{p}) \tag{40}$$

$$\begin{gathered} \boldsymbol{\mu}(\boldsymbol{\psi}) = \begin{bmatrix} \boldsymbol{\mu}_1(\boldsymbol{\psi}) \\ . \\ \boldsymbol{\mu}_j(\boldsymbol{\psi}) \\ . \\ \boldsymbol{\mu}_N(\boldsymbol{\psi}) \end{bmatrix}, \quad \boldsymbol{\mu}_j(\boldsymbol{\psi}) = \begin{bmatrix} . \\ . \\ \mu_{ij} \\ . \\ . \end{bmatrix}_{i \in \mathrm{A}_j \cup \mathrm{B}_j} \\ \boldsymbol{p} = \begin{bmatrix} \boldsymbol{p}_1 \\ . \\ \boldsymbol{p}_j \\ . \\ \boldsymbol{p}_N \end{bmatrix}, \quad \boldsymbol{p}_j = \begin{bmatrix} . \\ . \\ P_{ij} \\ . \\ . \end{bmatrix}_{i \in \mathrm{A}_j \cup \mathrm{B}_j} \\ \mu_{ij} = P_{0j} + 20 \log \left(\left[\frac{\lambda}{4\pi} \right] \times \left| \frac{\sqrt{G_l}}{l_{ij}} + \frac{R_{ij} \sqrt{G_r}\, e^{-j\Delta\varphi_{ij}}}{x_{ij} + x'_{ij}} \right| \right) \end{gathered} \tag{41}$$

Therefore, the CRLB for $\boldsymbol{\psi}$ is defined as

$$CRLB(\boldsymbol{\psi}) = diag\left(\mathrm{J}^{-1}(\boldsymbol{\psi})\right) \tag{42}$$

where $\mathrm{J}(\boldsymbol{\psi})$ is the Fisher information matrix

$$\mathrm{J}(\boldsymbol{\psi}) = \sigma^{-2}\left[\frac{\partial\, ln\, p(\boldsymbol{p},\boldsymbol{\psi})}{\partial \boldsymbol{\psi}}\right]^{T}\left[\frac{\partial\, ln\, p(\boldsymbol{p},\boldsymbol{\psi})}{\partial \boldsymbol{\psi}}\right] = \sigma^{-2}\boldsymbol{F}^{T}\boldsymbol{F} \tag{43}$$

$$\boldsymbol{F} = \frac{\partial \boldsymbol{\mu}(\boldsymbol{\psi})}{\partial \boldsymbol{\psi}} = \begin{bmatrix} \boldsymbol{F}_1 \\ . \\ \boldsymbol{F}_j \\ . \\ \boldsymbol{F}_N \end{bmatrix}, \qquad \boldsymbol{F}_j = \begin{bmatrix} . \\ . \\ \boldsymbol{f}_{ij} \\ . \\ . \end{bmatrix}_{i\in \mathrm{A}_j \cup \mathrm{B}_j}$$

$$\boldsymbol{f}_{ij} = \left[\frac{\partial \mu_{ij}(\boldsymbol{\psi})}{\partial x_j}, \qquad \frac{\partial \mu_{ij}(\boldsymbol{\psi})}{\partial y_j}, \qquad \frac{\partial \mu_{ij}(\boldsymbol{\psi})}{\partial P_{0\mathrm{j}}}\right] \tag{44}$$

$$\frac{\partial \mu_{ij}(\boldsymbol{\psi})}{\partial x_j} = \frac{\partial \mu_{ij}(\boldsymbol{\psi})}{\partial d_{ij}} \times \frac{\partial d_{ij}}{\partial x_j}, \qquad \frac{\partial \mu_{ij}(\boldsymbol{\psi})}{\partial y_j} = \frac{\partial \mu_{ij}(\boldsymbol{\psi})}{\partial d_{ij}} \times \frac{\partial d_{ij}}{\partial y_j}, \qquad \frac{\partial \mu_{i}(\boldsymbol{\psi})}{\partial P_{0\mathrm{j}}} = 1$$

$$\frac{\partial \mu_{ij}(\boldsymbol{\psi})}{\partial d_{ij}} \frac{10}{\ln(10) \times \left(\left(\frac{\sqrt{G_l}}{l_{ij}} + \frac{\sqrt{G_r} R_{ij}}{x_{ij} + x'_{ij}} \cos \Delta\varphi_{ij} \right)^2 + \left(\frac{\sqrt{G_r} R_{ij}}{x_{ij} + x'_{ij}} \sin \Delta\varphi_{ij} \right)^2 \right)}$$

$$\times \left(\left[2 \times \left(\frac{\sqrt{G_l}}{l_{ij}} + \frac{\sqrt{G_r} R_{ij}}{x_{ij} + x'_{ij}} \cos \Delta\varphi_{ij} \right) \right.\right.$$

$$\times \left(\sqrt{G_l} \left(\frac{-d_{ij}}{{l_{ij}}^3} \right) \right.$$

$$\left. + \sqrt{G_r} \left(\frac{-d_{ij}}{\left[x_{ij} + x'_{ij} \right]^3} \right) \cos \phi \times \frac{-\sin \Delta\varphi_{ij}}{x_{ij} + x'_{ij}} \right.$$

$$\left.\left. \times \left(\frac{2\pi}{\lambda} \left(\frac{d_{ij}}{\left(x_{ij} + x'_{ij} \right)} - \frac{d_{ij}}{l_{ij}} \right) \right) \right) \right] \qquad (45)$$

$$+ \left[2 \times \left(\frac{\sqrt{G_r} R_{ij}}{x_{ij} + x'_{ij}} \sin \Delta\varphi_{ij} \right) \right.$$

$$\times \left(\sqrt{G_r} \left(\frac{-d_{ij}}{\left[x_{ij} + x'_{ij} \right]^3} \right) \sin\ \Delta\varphi_{\mathrm{ij}} \times \frac{\cos \Delta\varphi_{ij}}{x_{ij} + x'_{ij}} \right.$$

$$\left.\left. \left. \times \left(\frac{2\pi}{\lambda} \left(\frac{d_{ij}}{\left(x_{ij} + x'_{ij} \right)} - \frac{d_{ij}}{l_{ij}} \right) \right) \right) \right] \right)$$

$$\frac{\partial d_{ij}}{\partial x_j} = \frac{-\left(a_i - x_j \right)}{d_{ij}} \qquad i \in \mathrm{A}_j$$

$$\frac{\partial d_{ij}}{\partial y_i} = \frac{-\left(b_i - y_j \right)}{d_{ij}} \qquad i \in \mathrm{A}_j$$

$$\frac{\partial d_{ij}}{\partial x_j} = \frac{-(x_i - x_j)}{d_{ij}} \qquad i \in B_j$$

$$\frac{\partial d_{ij}}{\partial y_i} = \frac{-(y_i - y_j)}{d_{ij}} \qquad i \in B_j$$

4.6 Numerical Results and Discussion

This section will discuss the performance of the proposed estimators for cooperative localizations for grid-based deployment and random-based deployment shown in Figure 5 and Figure 6. In this section, geophones assumed to have full connections with neighbor geophones and gateways within the cluster. The estimators that are used for cooperative localization are: MLE and SDP. WLS estimator cannot be used for cooperative localization since the model in (23) will be nonlinear if measurements between geophones included. SDP estimator in (39) is a convex optimization technique that converge to the global minima without initialization. However, MLE estimator in (38) is nonlinear and nonconvex. Therefore, initialization is required, and it is critical to the convergence to correct solution. We used SDP estimation as an initialization point for MLE estimator. MLE uses DE optimization algorithm as shown in Figure 12. The simulation parameters used are shown in Table 4.

Table 4: Simulation Parameters of Cooperative Localization

Simulation Parameter	**Value**
Average transmit power	10 dBm
h_t	0.8 (m)
h_r	1.5 (m)
f	470 MHz
G_l	1 dBi
G_r	1 dBi
ε	3.0000 - 0.0038i

Monte-Carlo simulations have been performed to observe the performance of the estimators for both grid-based deployment and random-based deployment. These estimators can be compared with CRLB which represents the minimum RMSE for any unbiased estimator. Figure 15 and Figure 16 show the Root-Mean-Square-Error (RMSE) verse the shadowing standard deviation (σ). The RMSE is calculated based on 200 noise measurements. The simulations results show that cooperation between nodes can enhance the localization error tremendously. SDP estimator has the lowest accuracy performance. However, it has the lowest computational complexity, and it does not require initialization step. It can be shown in Figure 15 and Figure 16 that RMSE between the SDP and MLE are close. It has been observed that RMSE is geometry dependent. The localization performance for grid deployment in Figure 16 is better than random deployment in Figure 15. We observed that the RMSE values for some estimators got lower than CRLB due to the fact that they are biased, and a limited number of measurements was considered. Therefore, estimators cannot be lower bounded by CRLB [35].

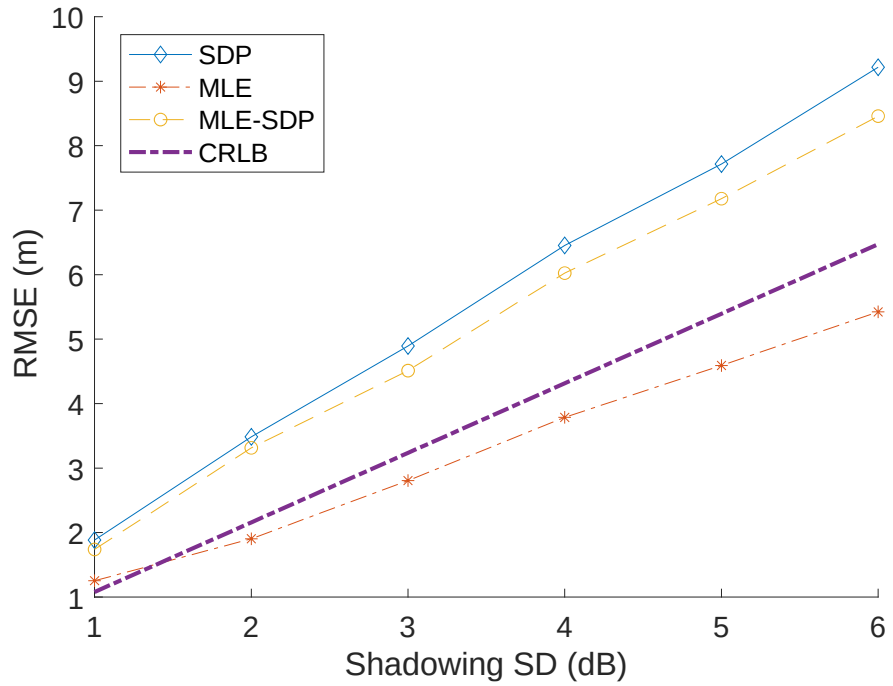

Figure 15: Cooperative localization performance for different estimators (Random-Based Deployment)

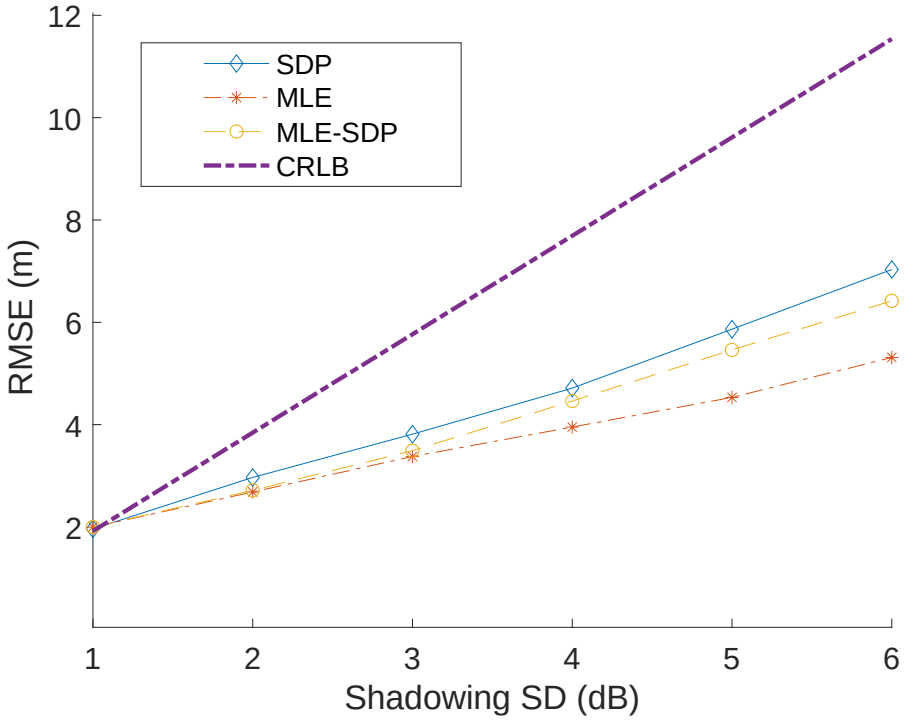

Figure 16: Cooperative localization performance for different estimators (Grid-Based Deployment)

4.6.1 Effect of Cooperative Nodes on Localization Accuracy

In previous section, we observed that full cooperation between geophones can result in a substantial localization error reduction. This section will study the effect of the number of cooperative nodes on localization accuracy for grid-based deployment and random-based deployment shown in Figure 17 and Figure 18.

Figure 17 and Figure 18 show that the effect of the number of cooperative nodes for random and grid deployments, respectively. The number of cooperative nodes is varied from 1 (noncooperative) until 10 (full cooperation). It is observed from both Figure 17 and Figure 18 that the number of cooperative nodes plays a major rule in localization accuracy. Furthermore, the RMSE values can be lower than CRLB since the estimators are biased.

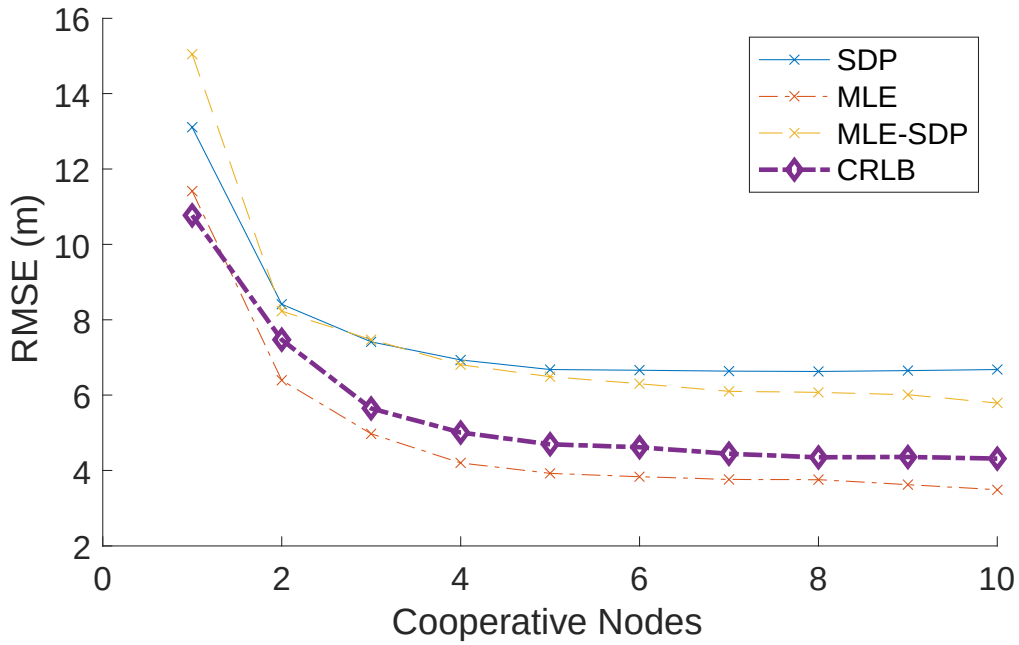

Figure 17: Effect of the number of cooperative nodes on localization accuracy (Random Deployment)

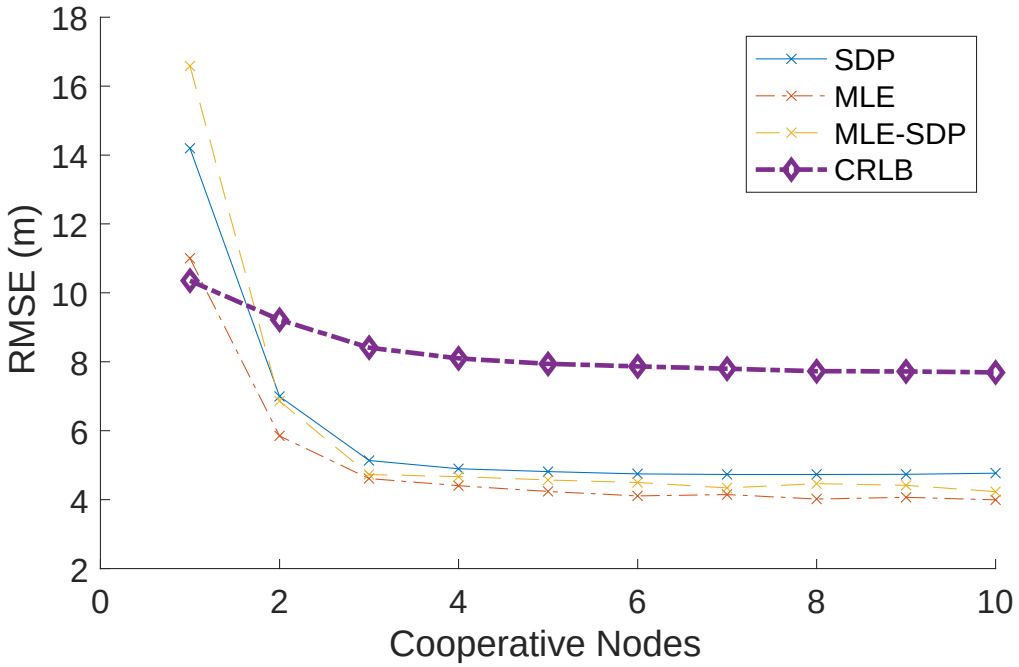

Figure 18: Effect of the number of cooperative nodes on localization accuracy (Grid Deployment)

4.6.2 Effect of Connections on Localization Accuracy

In subsection 4.6.1, we observed that the number of cooperative nodes can enhance the localization performance. It was assumed that each geophone is connected to all nearby gateways withing the cluster, while the number of connected geophones varied from 1-10. However, in seismic survey areas, it might occur that a set of geophones cannot make connection with any gateway due to obstacles between geophones and gateways. Therefore, we will study the effect when geophones are connected to the closest nodes, whether geophones or gateways. The number of connections will be varied from the closest 4 nodes to all nodes. It can be seen that it is possible to have a decent localization performance even if not all geophones are connected to the gateways within the cluster. It can be seen from Figure 19 and Figure 20 that the performance is stable when the number of connections exceeds 8.

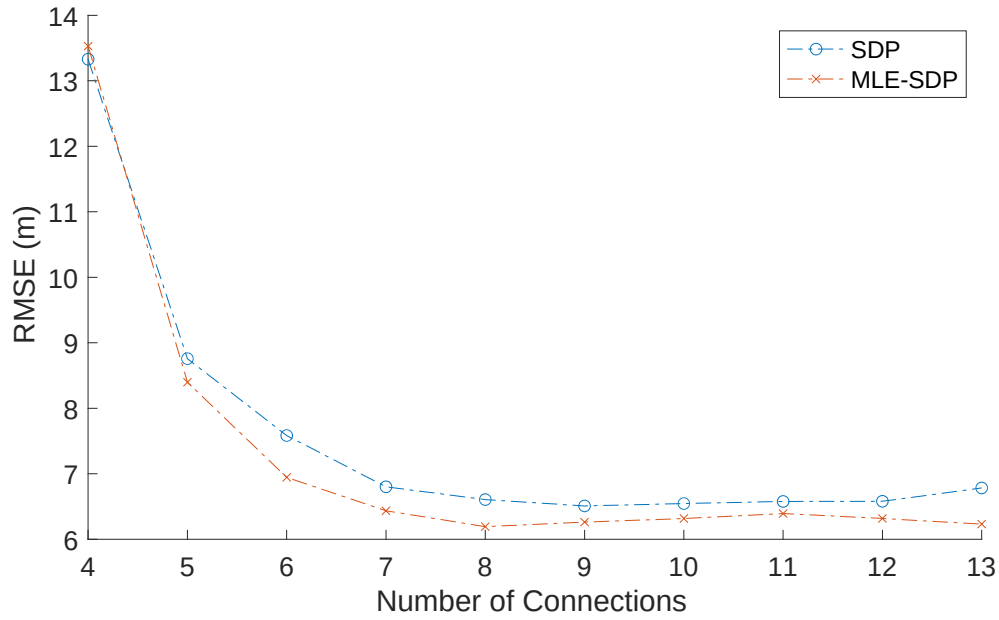

Figure 19: Effect of the number of connections on localization accuracy (Random Deployment)

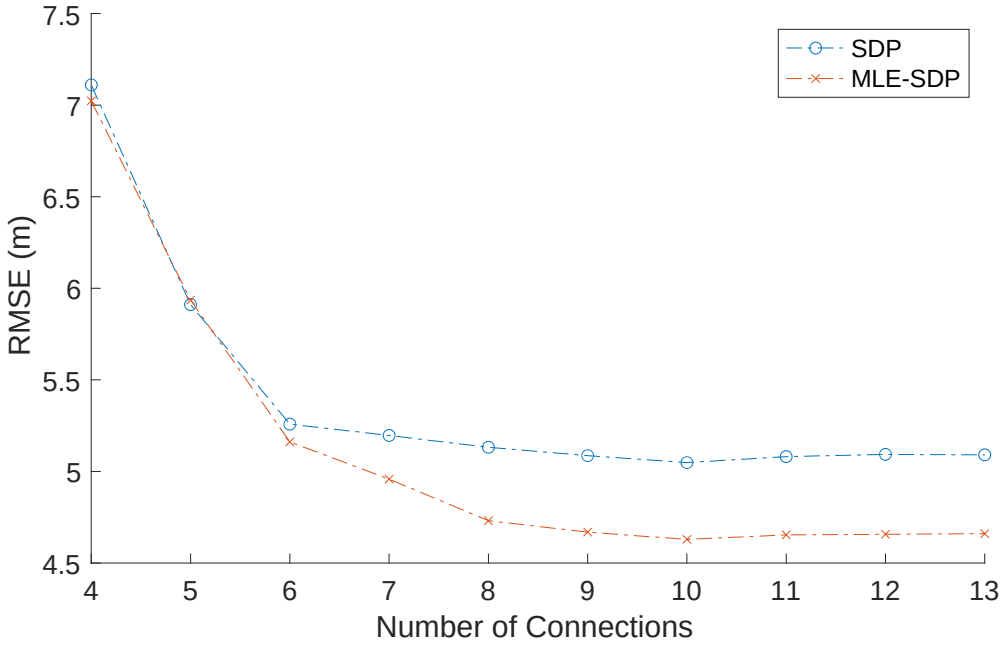

Figure 20: Effect of the number of connections on localization accuracy (Grid Deployment)

4.6.3 Effect of Antennas Heights on Localization Accuracy

Two-Ray pathloss model is an accurate model for seismic survey acquisition. This model is dependent on the antennas' heights and gains, carrier frequency and complex permittivity of the ground, as discussed in subsection 1.5.2. The received signal strength experiences a

severe constructive/destructive interference from the reflected wave when the distance between nodes d is less than the critical distance d_c. The critical distance is given by

$$d_c = \frac{4h_t h_r}{\lambda} \tag{46}$$

Therefore, the height of geophones (h_t) and gateways (h_r) can affect the localization accuracy when h_t and h_r result $d_c > d$. This section will study the effect of antennas heights for grid-based deployment and random-based deployment shown in Figure 5 and Figure 6. In Figure 21 and Figure 22, shows the localization performance using numerical simulations. The RMSE is calculated based on 500 noise realizations. The simulation parameters are shown in Table 5.

Table 5: Simulation Parameters for the Effects of Antennas Heights on Localization Accuracy

Simulation Parameter	**Value**
Average transmit power	10 dBm
h_t	(20 to 100) % of h_r (m)
h_r	1.5 (m) 2.5 (m) 3.5 m(m)
f	470 MHz
G_l	1 dBi
G_r	1 dBi
ε	3.0000 - 0.0038i
Shadowing standard deviation	4 dB

As can be shown in Figure 21 and Figure 22, as the geophones' antenna heights decrease, the localization performance enhance. The fluctuation in the performance is caused since the critical distance is higher than the distance between nodes $d_c > d$. At small gateways' heights i.e. ($h_r = 1.5$ to $2.5\ m$) the localization performance is more stable than at relatively higher heights i.e. ($h_r = 3.5\ m$). The fluctuation experienced more in grid deployment since the number of close nodes is higher than random deployment.

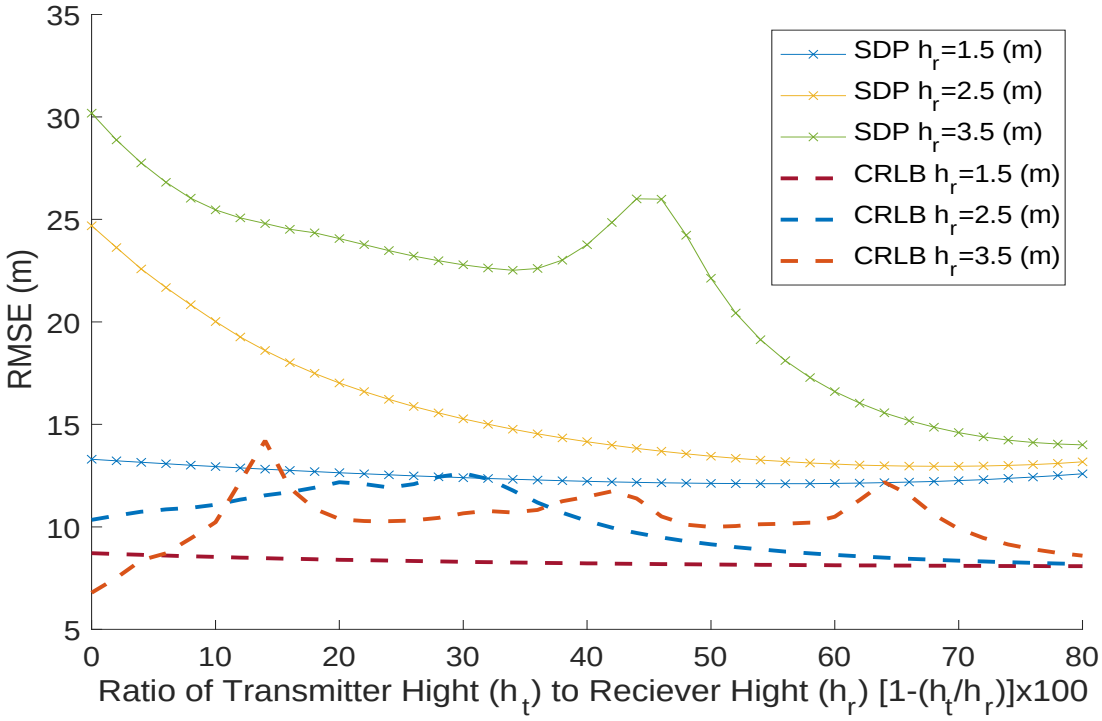

Figure 21: Effect of antennas heights on localization accuracy (Random Deployment)

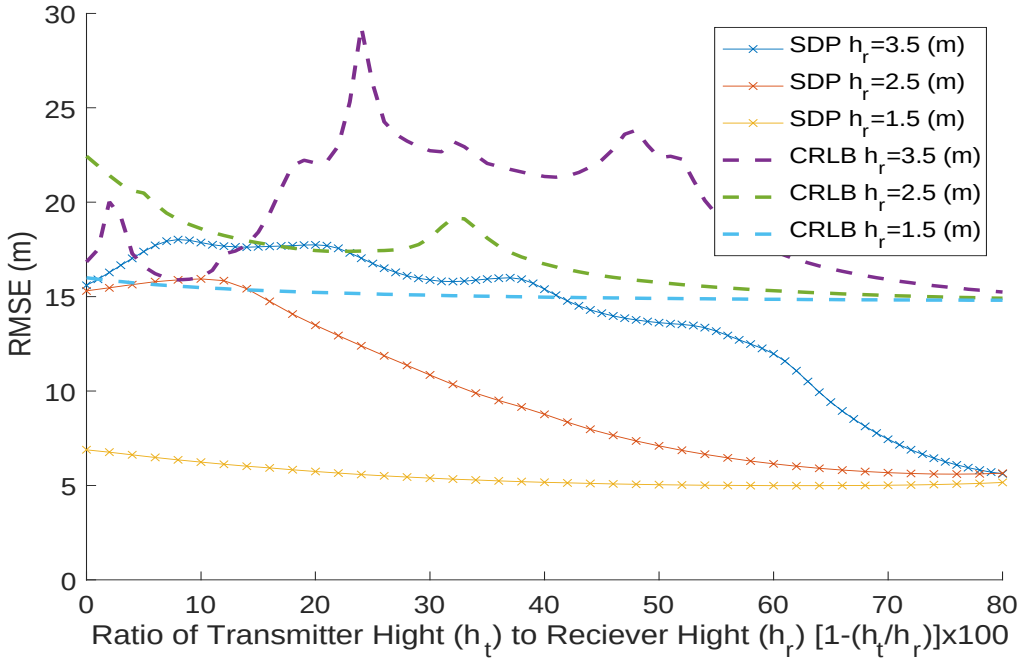

Figure 22: Effect of antennas heights on localization accuracy (Grid Deployment)

4.6.4 Effect of Antennas Gain on Localization Accuracy

As discussed earlier, Two-Ray pathloss model provide an accurate model for seismic survey acquisitions. One of the parameters that can affects the localization accuracy is the gains of antennas G_l and G_r. The antennas' gains are critical especially in the case when the transmitted power is unknown since the estimated power uncertainty will increase. This section will study the effect of antennas gain on localization accuracy for grid-based deployment and random-based deployment shown in Figure 5 and Figure 6. The simulation parameters are shown in Table 6.

Table 6: Simulation Parameters for the Effect of Antennas Gain on Localization Accuracy

Simulation Parameter	**Value**
Average transmit power	10 dBm
h_t	0.8 (m)
h_r	1.5 (m)
f	470 MHz
G_l	0.5-3 dBi
G_r	0.5-3 dBi
ε	3.0000 - 0.0038i
Shadowing standard deviation	4 dB

Figure 23 shows the numerical simulation for the localization accuracy by changing the antennas gains. The RMSE is calculated based on 500 noise realizations. As shown in Figure 23, the localization performance increase as both G_l and G_r increase up to a specific gain, but then decrease due to increasing antenna gain even though there is an uncertainty of the node location and transmitted power.

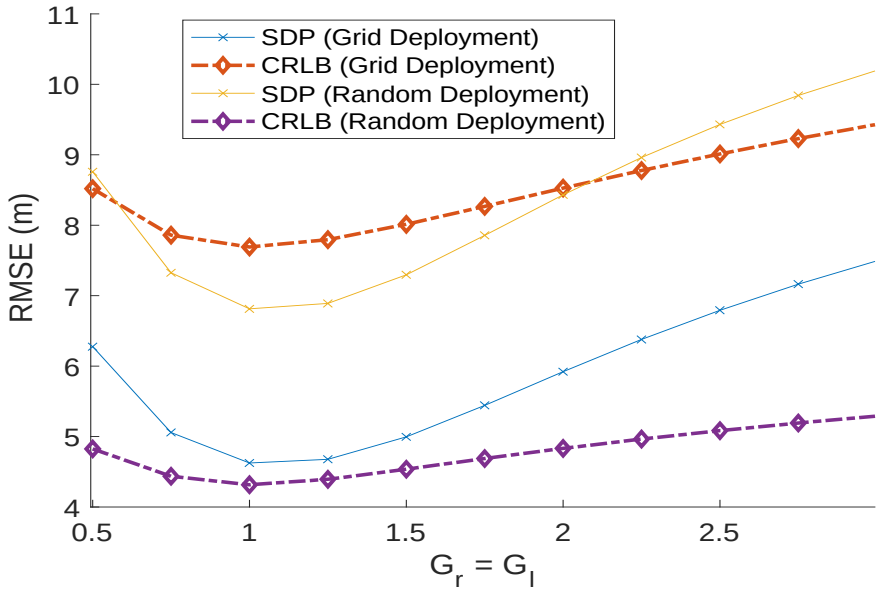

Figure 23: Effect of antennas gains on localization accuracy (Grid and Random Deployments)

4.6.5 Effect of Carrier Frequency on Localization Accuracy

This section will study the carrier frequency effect on localization performance. The carrier frequency is the inverse of the wavelength ($f = 1/\lambda$). The wavelength λ can affect d_c in (46) as d_c is directionally proportional to f. Therefore, increasing d_c is not desirable due to the constructive/destructive interference cased when $d_c > d$. The simulation parameters are shown in Table 7.

Table 7: Simulation Parameters for the Effect of Carrier Frequency on Localization Accuracy

Simulation Parameter	Value
Average transmit power	10 dBm
h_t	0.8 (m)
h_r	1.5 (m)
f	500-1000 MHz
G_l	1 dBi
G_r	1 dBi
ε	3.0000 - 0.0038i
Shadowing standard deviation	4 dB

Figure 24 shows the numerical simulation for localization accuracy for grid-based deployment and random-based deployment shown in Figure 5 and Figure 6. The RMSE is calculated based on 500 noise realizations. As shown in Figure 24 the localization error increase as the carrier frequency increases.

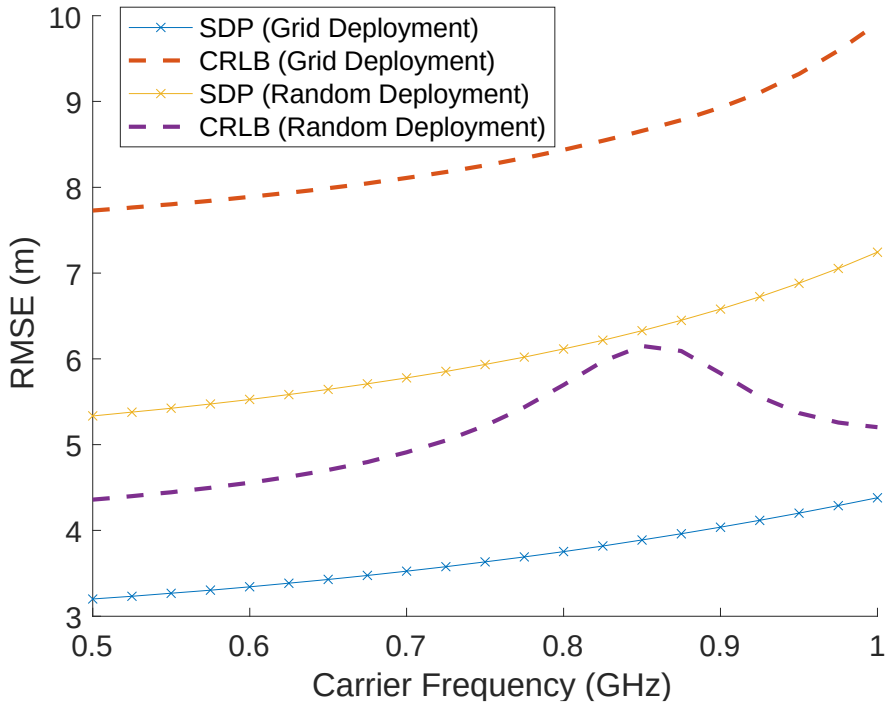

Figure 24: Effect of carrier frequency on localization accuracy (Grid and Random Deployments)

CHAPTER 5

Time of Arrival Localization Techniques for Seismic Surveys

In this chapter, we will discuss different TOA localization methods. Throughout this chapter, perfect synchronization will be assumed and NLOS mitigation technique will be discussed.

5.1 Introduction

Time of Arrival (TOA) localization technique is the method of localization where the ranging techniques used is the traveling time of signal between nodes [42], [43]. TOA localization tend to have higher accuracy than RSSI localization [16]. In RSSI localization, the shadowing and multipath effects can attenuate the signal heavy [12]. This can result a large localization error since the received signal strength is the ranging technique used. TOA localization, has similar localization principle with RSSI localization where it requires three noncolinear gateways in order to estimate the location [7]. In contrast, TOA localization does not estimate the distance between nodes based on the received signal strength. However, it utilizes the traveling time of the signal between nodes to estimate the distance and hence the location. Therefore, shadowing and multipath cannot affect the localization accuracy as long as the signal exceeds the receiver sensitivity threshold and can be decoded correctly. However, this localization accuracy enhancement come with a cost. In TOA, nodes need to be synchronized accurately to estimate the distances. The synchronization error will increase in a localization error [30]. Nodes' synchronization adds a computational complexity and energy overheads to the WSN. This what makes

RSSI preferable in WSN since geophones are limited in term of energy and processing capabilities. In addition to synchronization error, non-line-of-sight (NLOS) error can occur when there is no line-of-sight (LOS) between nodes which results a longer signal propagation time and hence localization error [30].

5.2 System Model

We will adopt the same notations conventions used in earlier chapters. Therefore, let i and j be the indices of i^{th} gateway and j^{th} geophone where $i \in \mathsf{C}$ and $j \in \mathcal{L}$. C is the set of indices of gateways, $\mathsf{C} = \{1,2,\dots,M\}$; and $\mathcal{L}$ is the set of indices of geophones, $\mathcal{L} = \{1,2,\dots,N\}$. Furthermore, let A_j and B_j be the set of indices of gateways and geophones connected to geophone j respectively, such that $\mathrm{A}_j \subseteq \mathsf{C}$ and $\mathrm{B}_j \subseteq \mathcal{L}$. Let $\boldsymbol{y} = [\boldsymbol{y}_1, \dots, \boldsymbol{y}_M]^T$, $\boldsymbol{x} = [\boldsymbol{x}_1, \dots, \boldsymbol{x}_N]^T$ be the set of the gateways and geophones 2-D coordinates respectively where $\boldsymbol{y}_i = [a_i, b_i]^T$ and $\boldsymbol{x}_j = \left[x_j, y_j\right]^T \in \mathbb{R}^2$. In this chapter we will consider only cooperative localization since noncooperative localization is a special case when $\mathrm{B}_j = \emptyset$. Let r_{ij} be the measured distance between j^{th} geophone and i^{th} node. Therefore, r_{ij} is given by

$$r_{ij} = \frac{t_{ij}}{c} \qquad i \in \mathrm{A}_j \cup \mathrm{B}_j \qquad (47)$$

where t_{ij} is the signal propagation time between node i and node j, $c \approx 3 \times 10^8$ is the speed of light [30]. Therefore, r_{ij} can be represented in a different form as follows

$$r_{ij} = \mathrm{d}_{ij} + n \qquad \text{for LOS} \quad (48)$$

$$r_{ij}^{*} = \mathrm{d}_{ij} + b_{ij} + n \qquad \text{for NLOS} \quad (49)$$

where $n \sim N(0, \sigma^2)$, $b_{ij} \geq 0$. b_{ij} is the bias caused by NLOS additional distance [20]. d_{ij} is the Euclidian distance between the nodes, which is given by

$$d_{ij} = \sqrt{\left(x_j - a_i\right)^2 + \left(y_j - b_i\right)^2} \qquad i \in \mathrm{A}_j \tag{50}$$

$$d_{mj} = \sqrt{\left(x_j - y_m\right)^2 + \left(y_j - y_m\right)^2} \qquad m \in \mathrm{B}_j$$

where the Additive-White-Gaussian Noise (AWGN) n is due to thermal noise at receivers.

5.3 Line-of-Sight Localization

In line-of-Sight (LOS) environment, all nodes are assumed to have a LOS between each other. In LOS localization, we will use the same estimators that has been used for RSSI based localization, which are: Maximum Likelihood Estimation (MLE), Semidefinite Programming (SDP) and Weighted Least Square (WLS).

5.3.1 Maximum Likelihood Estimation

Maximum Likelihood Estimation (MLE) is considered which approaches the CRLB asymptotically. From (48) the MLE for cooperative TOA localization is defined as

$$\hat{\mathbf{\Psi}} = \underset{[\boldsymbol{x}] \in \mathbb{R}^{2\mathrm{N}}}{\operatorname{argmin}} \sum_{j \in \mathcal{L}} \sum_{i \in \mathrm{A}_j \cup \mathrm{B}_j} \frac{1}{\sigma^2} \left[r_{ij} - d_{ij}\right]^2 \tag{51}$$

The model is non-convex and nonlinear. Therefore, nonlinear estimator needs to be used. As has been done with RSSI MLE, DE optimization was used. We will use the same optimization technique for (50).

5.3.2 Semidefinite Programming (SDP)

Semidefinite Programming (SDP) is a convex optimization tool that is known for its simplicity, robustness and fast convergence toward the global minima [44], [45]. The MLE

objective function (50) can be modified in order to make it convex. This can be done by using the epigraph method. Therefore, by introducing the auxiliary variable $\boldsymbol{z} = \boldsymbol{x}^{\boldsymbol{T}}\boldsymbol{x}$ and t_{ij}, (50) can be written as

$$\underset{[\boldsymbol{x},\boldsymbol{z},h_{ij},d_{\mathrm{ij}},t_{ij}]}{\text{minimize}} \sum_{j\in\mathcal{L}} \sum_{i\in \mathrm{A}_j \cup \mathrm{B}_j} \frac{1}{\sigma^2} t_{ij} \tag{52}$$

subject to

$$t_{ij} = h_{ij} - \mathrm{r}_{ij}\,\mathrm{d}_{ij} \qquad i \in \mathrm{A}_j \cup \mathrm{B}_j$$

$$h_{ij} = \begin{bmatrix} \boldsymbol{y}_i \\ -\mathbf{e}_j \end{bmatrix}^T \begin{bmatrix} \boldsymbol{I}_2 & \boldsymbol{x} \\ \boldsymbol{x}^T & \boldsymbol{z} \end{bmatrix} \begin{bmatrix} \boldsymbol{y}_i \\ -\mathbf{e}_j \end{bmatrix} \qquad i \in \mathrm{A}_j$$

$$h_{ij} = \begin{bmatrix} \mathbf{0}_2 \\ \mathbf{e}_i - \mathbf{e}_j \end{bmatrix}^{\boldsymbol{T}} \begin{bmatrix} \boldsymbol{I}_2 & \boldsymbol{x} \\ \boldsymbol{x} & \boldsymbol{z} \end{bmatrix} \begin{bmatrix} \mathbf{0}_2 \\ \mathbf{e}_i - \mathbf{e}_j \end{bmatrix} \qquad i \in \mathrm{B}_j$$

$$\begin{bmatrix} h_{ij} & d_{ij} \\ d_{ij} & \mathbf{1} \end{bmatrix} = \mathbf{0}_2 \qquad i \in \mathrm{A}_j$$

$$\begin{bmatrix} \boldsymbol{I}_2 & \boldsymbol{x} \\ \boldsymbol{x}^T & \boldsymbol{z} \end{bmatrix} = \mathbf{0}_{N+2}$$

where $\mathbf{e}_j$ is a vector of zeros except at the j^{th} entry is a one. In order to make (52) convex, the last two equality constrains can be relaxed into inequality constrains as follow.

$$\begin{bmatrix} h_{ij} & d_{ij} \\ d_{ij} & \mathbf{1} \end{bmatrix} \succcurlyeq \mathbf{0_2} \qquad i \in \mathrm{A}_j$$

$$\begin{bmatrix} \boldsymbol{I_2} & \boldsymbol{x} \\ \boldsymbol{x^T} & \boldsymbol{z} \end{bmatrix} \succcurlyeq \mathbf{0}_{N+2}$$

Therefore, now we can use SDP to solve (52) after relaxation [46], [47].

5.3.3 Weighted Least Square

Weighted least Square (WLS) is characterized by its simplicity and low complexity [48]. WLS for TOA localization will be discussed in this section. Let $\boldsymbol{\theta}_j = [\boldsymbol{x}_j^T, \mathrm{s}_j]$, where $s = \boldsymbol{x}_j^T \boldsymbol{x}_j$. Then (48) can be written in an alternative for as follows

$$\boldsymbol{\theta}_j = \boldsymbol{h}_j + \boldsymbol{\epsilon}_{ij} \tag{53}$$

where

$$\boldsymbol{G}_j = \begin{bmatrix} \vdots \\ 2\boldsymbol{y}_i^T \quad -1 \\ \vdots \end{bmatrix}, \qquad \boldsymbol{h}_j = \begin{bmatrix} \vdots \\ \boldsymbol{y}_i^T \boldsymbol{y}_i - r_{ij}^2 \\ \vdots \end{bmatrix}, \qquad \boldsymbol{\epsilon}_{ij} = \begin{bmatrix} \vdots \\ \epsilon_{ij} \\ \vdots \end{bmatrix} \tag{54}$$

(53) is in a linear form. Therefore, WLS estimator can be used to estimate $\boldsymbol{\theta}_j$. LLS for (53) is given by

$$\widehat{\boldsymbol{\theta}}_j = \left(\boldsymbol{G}_j{}^T \boldsymbol{W}_j \boldsymbol{G}_j\right)^{-1} \boldsymbol{G}_j{}^T \boldsymbol{W}_j \boldsymbol{h}_j \tag{55}$$

where $\boldsymbol{W}_j = \sigma^{-2}\mathbf{I}_{|\mathrm{A}_j|}$.

5.4 Non-Line-of-Sight Localization

In Non-of-line-of-Sight (NLOS) environment, some nodes might not have a direct LOS between each other. Therefore, signal propagation time will be larger than the case of LOS. This additional propagation time will cause an estimation error. In the literature, most of the NLOS localization techniques rely on the fact that the nodes can distinguish NLOS from LOS [30], [49]–[51]. This might not practice in real scenario. Therefore, this section will discuss the analysis of NLOS localization by assuming all nodes have NLOS connection with each other. For NLOS localization, MLE derivations will not be possible due to the presence of the positive bias b_{ij}, which has unknown distribution. Therefore, we will use the nonlinear WLS for NLOS localization. The nonlinear WLS can be relaxed into

a convex optimization problem and solved by SDP estimator. The analysis will be discussed in the next section.

5.4.1 Semidefinite Programming

In this section, the derivations for nonlinear WLS will be discussed. Then, the nonlinear WLS can be relaxed into a convex optimization problem and solved by SDP. From (49), by squaring both sides of the equation, this will result in the following

$$\begin{aligned} {r_{ij}^*}^2 &= \left(d_{ij} + b_{ij} + n_{ij}\right)^2 \\ &= d_{ij}^2 + c_{ij} + \epsilon_{ij} + n_{ij}^2 \end{aligned} \tag{56}$$

where $\epsilon_{ij} = 2n_{ij}\left(d_{ij} + b_{ij}\right)$, $c_{ij} = b_{ij}^2 + 2b_{ij}d_{ij}$. For sufficiently small noise n_{ij}^2 can be neglected. Therefore,

$${r_{ij}^*}^2 \approx d_{ij}^2 + c_{ij} + \epsilon_{ij} \tag{57}$$

Therefore, we can estimate the unknown parameters using WLS as follows

$$\underset{[\boldsymbol{x_j}, b_{ij}]}{\text{minimize}} \sum_{j \in \mathcal{L}} \sum_{i \in \mathrm{A}_j \cup \mathrm{B}_j} \frac{1}{w_{ij}} \left({r_{ij}^*}^2 - d_{ij}^2 - c_{ij}\right)^2 \tag{58}$$

subject to

$$c_{ij} = b_{ij}^2 + 2b_{ij}d_{ij}$$

$${r_{ij}^*}^2 + u_{ij} \succcurlyeq d_{ij}^2$$

where $w_{ij} = \left(d_{ij} + b_{ij}\right)^{-2}\sigma^{-2} \approx {r_{ij}^*}^2\sigma^{-2}$, $u_{ij} = 2\sqrt{4\left(d_{ij} + b_{ij}\right)^2\sigma^2} \approx 2\sqrt{4\,{r_{ij}^*}^2\sigma^2}$

By introducing the auxiliary variable $\boldsymbol{z} = \boldsymbol{x}^T\boldsymbol{x}$ and relax the equality constrains into inequality constrains, the cooperative SDP is defined as

$$\underset{[\boldsymbol{x}, \boldsymbol{z}, h_{ij}, \alpha_{0\mathrm{j}}]}{\text{minimize}} \sum_{j \in \mathcal{L}} \sum_{i \in \mathrm{A}_j \cup \mathrm{B}_j} \left({r_{ij}^*}^2 - h_{ij} + c_{ij}\right)^2$$

subject to

$$h_{ij} = \begin{bmatrix} \boldsymbol{y}_i \\ -\mathbf{e}_j \end{bmatrix}^T \begin{bmatrix} \boldsymbol{I}_2 & \boldsymbol{x} \\ \boldsymbol{x}^T & \boldsymbol{z} \end{bmatrix} \begin{bmatrix} \boldsymbol{y}_i \\ -\mathbf{e}_j \end{bmatrix} \qquad i \in \mathrm{A}_j$$

$$h_{ij} = \begin{bmatrix} \mathbf{0_2} \\ \mathbf{e}_i - \mathbf{e}_j \end{bmatrix}^T \begin{bmatrix} \boldsymbol{I}_2 & \boldsymbol{x} \\ \boldsymbol{x} & \boldsymbol{z} \end{bmatrix} \begin{bmatrix} \mathbf{0}_2 \\ \mathbf{e}_i - \mathbf{e}_j \end{bmatrix} \qquad i \in \mathrm{B}_j$$

$$\begin{bmatrix} \boldsymbol{I}_2 & \boldsymbol{x}_j - \boldsymbol{y}_i \\ \boldsymbol{x}_j - \boldsymbol{y}_i & r_{ij}^{*\,2} + u_{ij} \end{bmatrix} \succcurlyeq \mathbf{0_2} \qquad i \in \mathrm{A}_j$$

$$\begin{bmatrix} \boldsymbol{I}_2 & \boldsymbol{x} \\ \boldsymbol{x}^T & \boldsymbol{z} \end{bmatrix} \succcurlyeq \mathbf{0}_{N+2}, \;\; c_{ij} \succcurlyeq 0 \; i \in \mathrm{A}_j \cup \mathrm{B}_j \qquad (59)$$

5.5 Cramér Rao Lower Bound Derivation

Cramér-Rao Lower Bound (CRLB) is defined as the lower limit of the variance of any unbiased estimator. It provides an insight about the estimators performance for different number of gateways and geophones [52]. In this section, the CRLB for TOA localization with unknown transmitted power will be derived. The CRLB main derivations for both RSSI and TOA are similar since the added noise is Gaussian and therefore their maximum likelihood functions will be similar. Let $\boldsymbol{\psi} = [\boldsymbol{x}]$, then the log ML function is defined as

$$\ln p(\boldsymbol{r}, \boldsymbol{\psi}) = k - \sigma^2 (\boldsymbol{\mu}(\boldsymbol{\psi}) - \boldsymbol{r})^T (\boldsymbol{\mu}(\boldsymbol{\psi}) - \boldsymbol{r}) \qquad (60)$$

$$\boldsymbol{\mu}(\boldsymbol{\psi}) = \begin{bmatrix} \boldsymbol{\mu}_1(\boldsymbol{\psi}) \\ . \\ \boldsymbol{\mu}_j(\boldsymbol{\psi}) \\ . \\ \boldsymbol{\mu}_N(\boldsymbol{\psi}) \end{bmatrix}, \quad \boldsymbol{\mu}_j(\boldsymbol{\psi}) = \begin{bmatrix} . \\ . \\ \mu_{ij} \\ . \\ . \end{bmatrix}_{i \in \mathrm{A}_j \cup \mathrm{B}_j}$$

$$\boldsymbol{p} = \begin{bmatrix} \boldsymbol{r}_1 \\ . \\ \boldsymbol{r}_j \\ . \\ \boldsymbol{r_N} \end{bmatrix}, \quad \boldsymbol{r}_j = \begin{bmatrix} . \\ . \\ r_{ij} \\ . \\ . \end{bmatrix}_{i \in \mathrm{A}_j \cup \mathrm{B}_j} \qquad (61)$$

$$\mu_{ij} = d_{ij}$$

Therefore, the CRLB for $\boldsymbol{\psi}$ is defined as

$$CRLB(\boldsymbol{\psi}) = diag\left(\mathrm{J}^{-1}(\boldsymbol{\psi})\right) \qquad (62)$$

where $\mathrm{J}(\boldsymbol{\psi})$ is the Fisher information matrix

$$\mathrm{J}(\boldsymbol{\psi}) = \sigma^{-2}\left[\frac{\partial\, ln\, p(\boldsymbol{r},\boldsymbol{\psi})}{\partial \boldsymbol{\psi}}\right]^{T}\left[\frac{\partial\, ln\, p(\boldsymbol{r},\boldsymbol{\psi})}{\partial \boldsymbol{\psi}}\right] = \sigma^{-2}\boldsymbol{F}^{\boldsymbol{T}}\boldsymbol{F} \tag{63}$$

$$\boldsymbol{F} = \frac{\partial \boldsymbol{\mu}(\boldsymbol{\psi})}{\partial \boldsymbol{\psi}} = \begin{bmatrix} \boldsymbol{F}_1 \\ . \\ \boldsymbol{F}_j \\ . \\ \boldsymbol{F}_N \end{bmatrix}, \qquad \boldsymbol{F}_j = \begin{bmatrix} . \\ . \\ \boldsymbol{f}_{ij} \\ . \\ . \end{bmatrix}_{i\in \mathrm{A}_j \cup \mathrm{B}_j}$$

$$\boldsymbol{f_{ij}} = \left[\frac{\partial \mu_{ij}(\boldsymbol{\psi})}{\partial x_j}, \qquad \frac{\partial \mu_{ij}(\boldsymbol{\psi})}{\partial y_j}\right] \tag{64}$$

$$\frac{\partial \mu_{ij}(\boldsymbol{\psi})}{\partial x_j} = \frac{\partial d_{ij}}{\partial x_j}, \qquad \frac{\partial \mu_{ij}(\boldsymbol{\psi})}{\partial y_j} = \frac{\partial d_{ij}}{\partial y_j}$$

$$\frac{\partial d_{ij}}{\partial x_j} = \frac{-(a_i - x_j)}{d_{ij}} \qquad i \in \mathrm{A}_j \tag{65}$$

$$\frac{\partial d_{ij}}{\partial y_i} = \frac{-(b_i - y_j)}{d_{ij}} \qquad i \in \mathrm{A}_j$$

$$\frac{\partial d_{ij}}{\partial x_j} = \frac{-(x_i - x_j)}{d_{ij}} \qquad i \in B_j$$

$$\frac{\partial d_{ij}}{\partial y_i} = \frac{-(y_i - y_j)}{d_{ij}} \qquad i \in B_j$$

5.6 Numerical Results and Discussion

This section will study the TOA localization performance. In this chapter, we will consider only cooperative localization since noncooperative localization is basically a special case when $B_j = \emptyset$. Furthermore, only LOS will be considered since in it is the case in land seismic acquisition. TOA model in (51), (52) and (53) does not depend on the antennas' heights or gains. Furthermore, the carrier frequency does not affect the localization performance. Therefore, their effects will not be studied in this chapter.

5.6.1 Effect of Cooperating Nodes on Localization Accuracy

This section will study TOA localization and the effect of the number of cooperative nodes in localization accuracy for grid-based and random-based deployments as shown in Figure 25 and Figure 26. It can be shown in Figure 25 and Figure 26 that the effect of the number of cooperative nodes for grid and random deployments, respectively. The number of cooperative nodes is varied from 1 (noncooperative) until 10 (full cooperation). It can be shown from Figure 25 and Figure 26 that the number of cooperative nodes plays a major rule in localization accuracy. SDP outperformed MLE even when MLE initiated by SDP solution. In term of optimization, MLE has lower objective function value than SDP. However, due to the AWGN, the global minimum might not result in the correct solution. The difference between the global minima and the correct solution depends on the level of the AWGN.

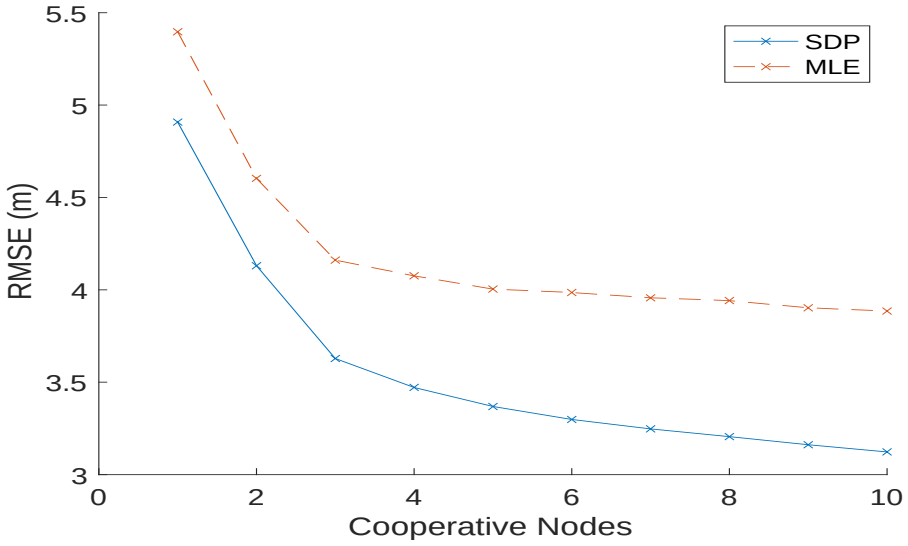

Figure 25: Effect of the number of cooperating nodes on localization accuracy (Grid-Deployment)

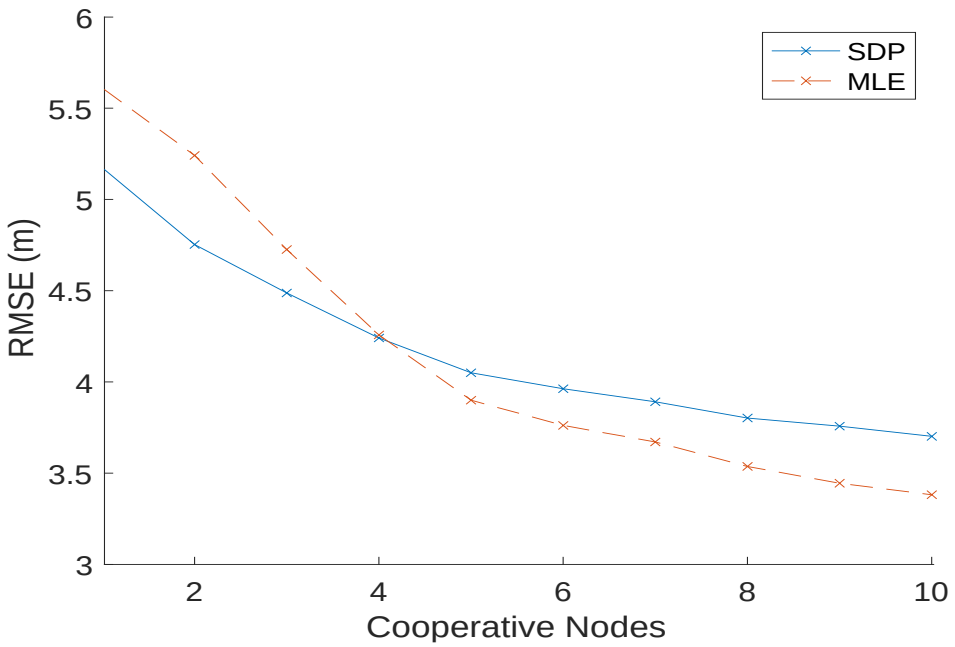

Figure 26: Effect of the number of cooperating nodes on localization accuracy (Random Deployment)

5.6.2 Effect of Connections on Localization Accuracy

In the previous section, it was seen that the number of cooperative nodes can enhance the localization performance. It was assumed that each geophone is connected to all nearby gateways withing the cluster, while the number of connected geophones varied from 1-10. However, in seismic survey areas, it might occur that a set of geophones cannot make connection with any gateways due to obstacles between geophones and gateways. Therefore, we will study the effect when geophones are connected to the closest nodes, whether geophones or gateways. The number of connections will be varied from the closest 4 nodes to all nodes, which is full cooperative. It can be seen that it is possible to have a decent localization performance even if not all geophones are connected to the gateways within the closer. It can be seen from Figure 27 and Figure 28 that the performance of the estimators enhances as the number of connections increase.

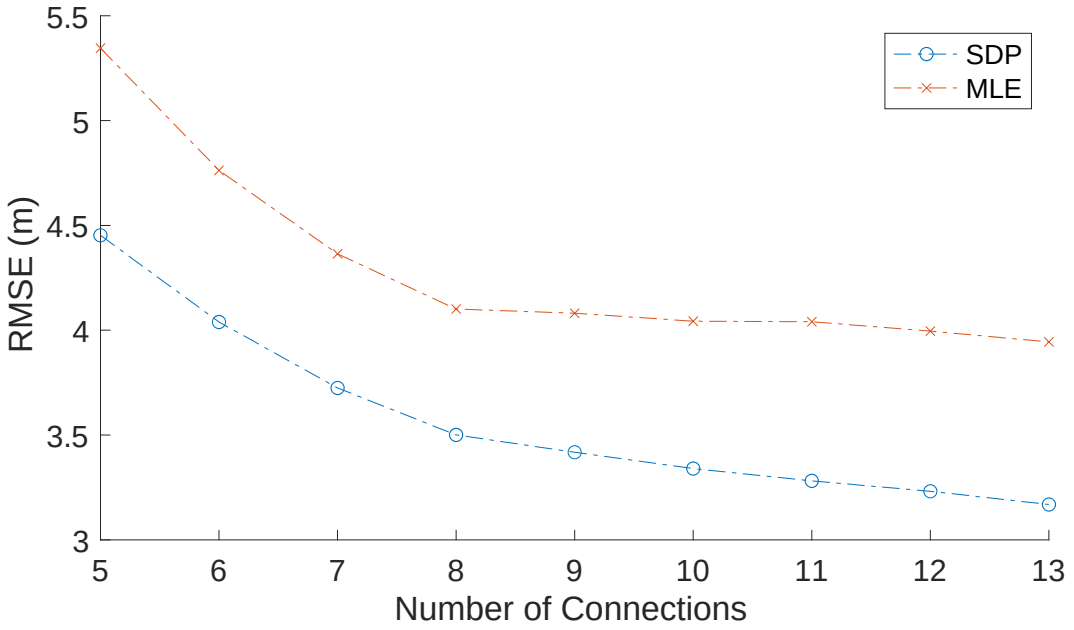

Figure 27: Effect of the number of connections on localization accuracy (Grid Deployment)

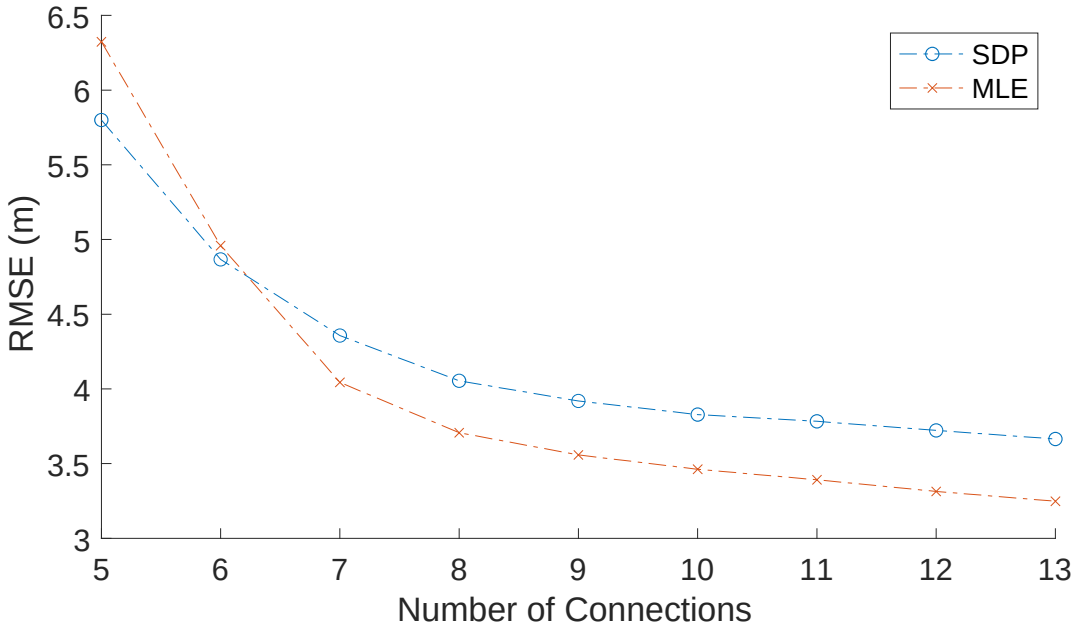

Figure 28: Effect of the number of connections on localization accuracy (Random Deployment)

5.6.3 Noncooperative vs Cooperative Localization

In this section, we will discuss and compare noncooperative localization with cooperative localization. As can be shown in Figure 29 and Figure 30, cooperative localization can

significantly enhance the localization performance. This is due to the increase of the number of measurements which will result in accurate positioning of geophones. Cooperative localization will add a complexity in the localization process. However, its advantages overweight its additional complexity. For instance, in a grid-deployment network under shadowing of 4 dB standard deviation, the cooperative localization with SDP has RMSE of around 2.6 m, while using SDP in noncooperative localization results in RMSE of 13 m. The accuracy deteriorates even more if we use the WLS technique in noncooperative localization at same shadowing conditions leading to an RMSE of 30 m. Hence, cooperative localization can improve the accuracy by 80% compared to the noncooperative case and by 91.3% compared to WLS under the grid-deployment.

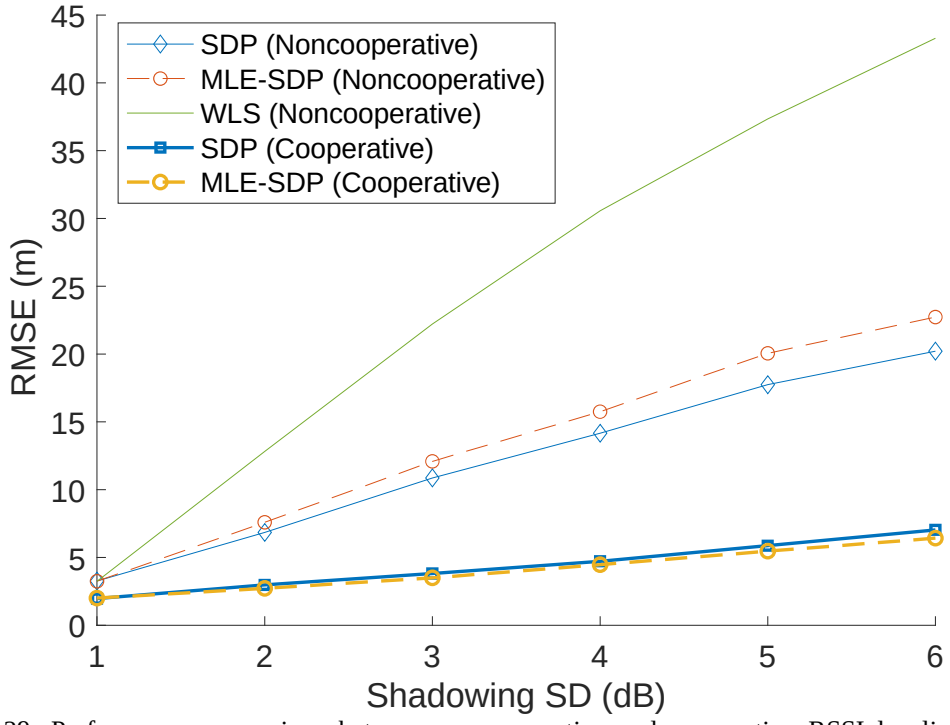

Figure 29: Performance comparison between noncooperative and cooperative RSSI localization (Grid Deployment)

Similarly, if the geophones are randomly deployed in the survey area the RMSE comparisons for the various localization techniques are shown in Figure 30. At shadowing with standard deviation of 4 dB, the SDP cooperative localization has an RMSE of around 4 m, while using SDP in noncooperative localization it results in loss of accuracy and RMSE is 10 m. This indicates an improvement of 60% in the localization accuracy when cooperative technique is implemented compared to the noncooperative case. Such improvement variation depends on the deployment of the network, and the cooperative localization always provide an improved accuracy. This improvement is substantial compared to the WLS in noncooperative setup which reaches 92%.

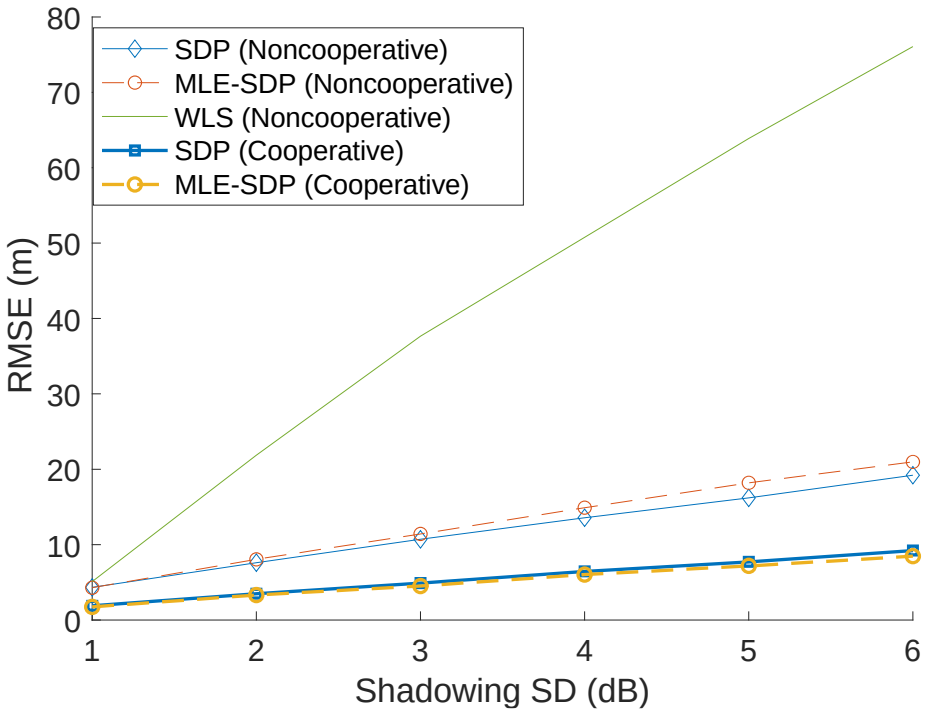

Figure 30: Performance comparison between noncooperative and cooperative RSSI localization (Random Deployment)

5.6.4 TOA vs RSSI Localization

ToA localization can provide better accuracy compared to RSSI localization. However, this comes with the expense of adding a computational and energy overhead in the WGN

due to the need of accurate synchronization between all elements in the network. Figure 31 and Figure 32 show a comparison between RSSI cooperative localization and TOA cooperative localization. It is clearly shown that TOA can provide better performance compared to RSSI localization. The gap can be seen clearly in Random topology. RSSI has a low complexity since it does not require synchronization; yet it provides a comparable performance to TOA localization. Specifically, at shadowing level of 4 dB, the RMSE in the cooperative SDP with RSSI is around 4.25 m, while it is 2.5 m in cooperative TOA localization. This indicates an improvement of 41.1% which is comparable given the complexity and synchronization associated with TOA localizations in general.

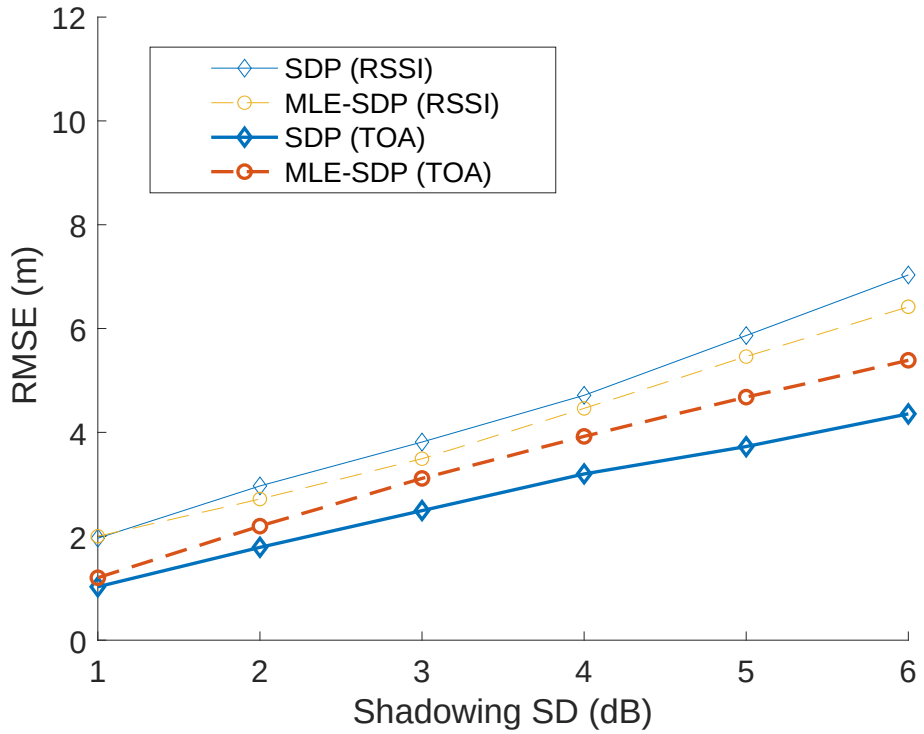

Figure 31: Performance comparison between cooperative RSSI and TOA localization (Grid Deployment)

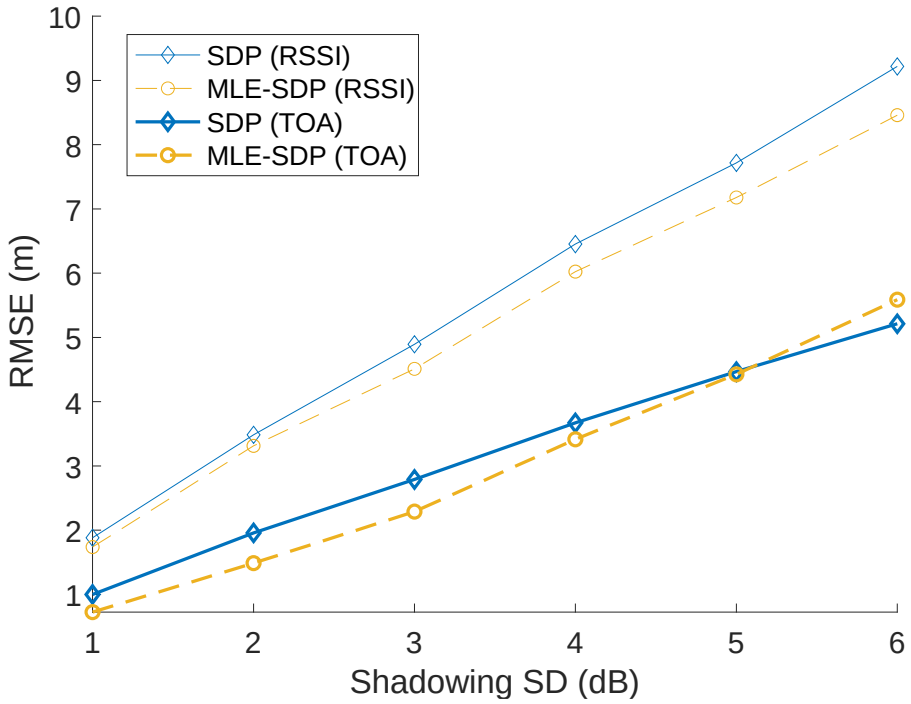

Figure 32: Performance comparison between cooperative RSSI and TOA localization (Random Deployment)

5.6.5 Two-Ray vs Log-Distance Propagation Models

In this section, we will discuss and show a comparison between localization using Two-Ray propagation model and Log-Distance propagation model. Log-Distance propagation model is a generic model and simple. It is widely used since it captures the signal propagation pattern for large range of environments. However, in WGN the signal experience strong interference from ground reflection due to small antennas size, which might affect the signal strength heavily. Therefore, Two-Ray Model is suitable for this environment. Figure 33 and Figure 34 show the localization performance for the proposed estimator using Two-Ray and Log-Distance propagation models. We can clearly see that the performance using Two-Ray propagation models is different than Log-Distance propagation model for both grid and random deployments. This is due to the fact that Two-

Ray propagation model accounts for the ground reflection effect, carrier frequency, antennas heights and gains in the localization process.

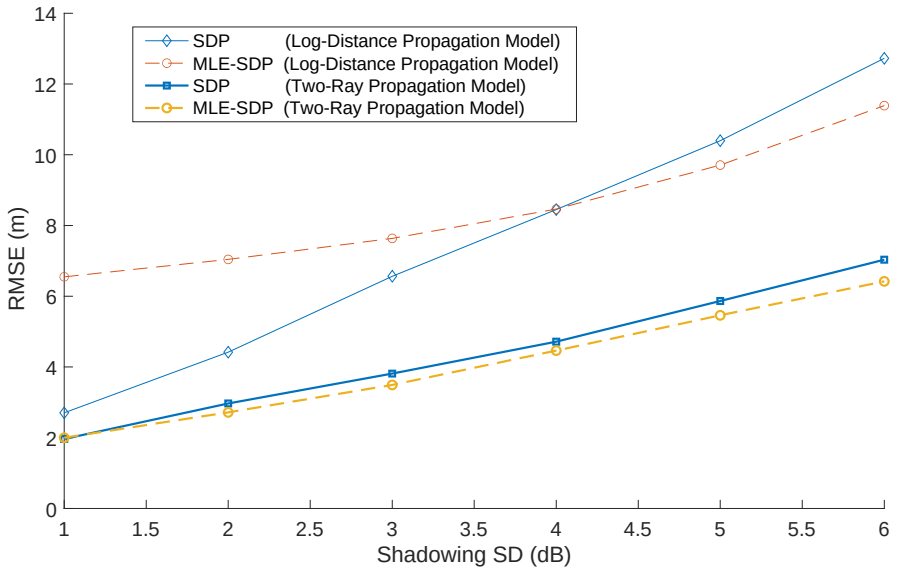

Figure 33: Performance comparison between cooperative RSSI localization using Two-Ray and Log-Distance propagation models (Grid Deployment)

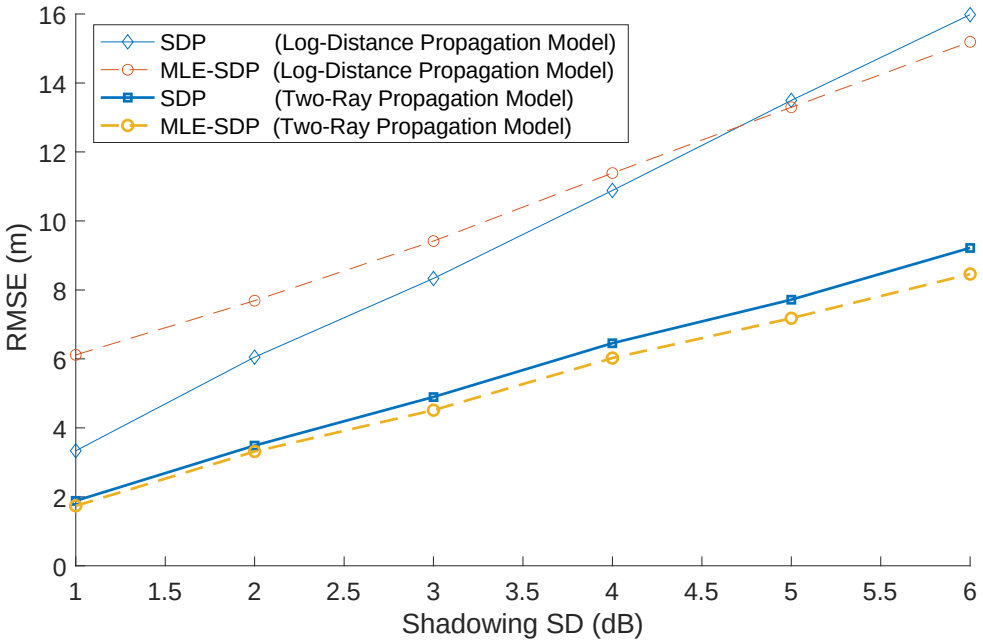

Figure 34:Performance comparison between cooperative RSSI localization using Two-Ray and Log-Distance propagation models (Random Deployment)

CHAPTER 6

CONCLUSIONS AND FUTURE WORK

This thesis discussed the localization techniques in wireless geophone networks for high-density seismic acquisition. The pathloss models in the literature are inapplicable to the geophones in a realistic seismic acquisition surveys due to ground reflection dominant multipath component. Therefore, the aim in this thesis is to tackle the inaccuracy of the pathloss model in the literature and provide a comprehensive analysis of localization performance using the proposed pathloss model, i.e. Two-Ray Pathloss model. Unlike most of the localization analysis and techniques, this thesis proposed RSSI localization techniques without a prior knowledge of the transmitted power at geophones.

We discussed the noncooperative localization, which is the classical method of localization, then the model was extended to cooperative localization without the knowledge of the transmitted power at geophones. Different location estimators were proposed, and different optimization methods were used. The performance of the estimators was investigated both theoretically and through simulations. It was shown that cooperative localization has a great impact on the localization accuracy. Furthermore, it was shown that as the number of cooperative nodes increases the localization accuracy increases. The scenario when a set of geophones cannot be connected to gateways was studied and the localization performance was satisfactory, and it was comparable to the cooperative case. The other parameters of the WGN such

as the antennas' heights and gains and the carrier frequency were investigated and it was found that these paraments can affect the localization performance and hence by proper selection of these parameters, localization performance can be enhanced substantially. Finally, the analysis of TOA localization was studied under both assumptions of LOS and NLOS. It was shown that TOA can have a better accuracy, however, this will come with a complexity overhead on the whole WGN since accurate synchronization is needed.

Future Work

We discussed in this thesis noncooperative and cooperative RSSI localization with unknown transmitted power using Two-Ray propagation model and showed the effect of pathloss parameters on localization accuracy. This model is suitable for near-ground signal propagation. The proposed models provide accurate energy-efficient localization methods. We plan to extend the accomplished work and enhance the localization performance by incorporating different ranging techniques such as TOA, TDOA and AOA with RSSI. Furthermore, multiple smart geophones, which are equipped with GPS capabilities, can be deployed to support the gateways in the localization process and enhance the localization performance. Finally, different simplified pathloss models, such as multi-slope pathloss model, can result in a simplified objective function for the localization and hence less computational complexity.

APPENDIX

APPNEDIX A: Semidefinite Programing Relaxation Derivations

Let A_j and B_j be the set of gateways and geophones connected to j^{th} geophone respectively, such that $A_j \subseteq \mathbb{C}$ and $B_j \subseteq \mathcal{L}$. Let $\boldsymbol{y} = [\boldsymbol{y}_1, \dots, \boldsymbol{y}_M]^T$, $\boldsymbol{x} = [\boldsymbol{x}_1, \dots, \boldsymbol{x}_N]^T$ be the set of the gateways and geophones 2-D coordinates respectively where $\boldsymbol{y}_i = [a_i, b_i]^T$ and $\boldsymbol{x}_j = \left[x_j, y_j\right]^T \in \mathbb{R}^2$. Let $\boldsymbol{p_0} = \left[P_{01}, P_{0j}, \dots, P_{0N}\right]^T$ denote geophones' transmitted power (in dBm) respectively. The received signal strength (in dBm) at i^{th} gateway from j^{th} geophone is given by

$$P_{ij} = P_{0j} + 20\log\left(\left[\frac{\lambda}{4\pi}\right] \times \left|\frac{\sqrt{G_l}}{l_{ij}} + \frac{R_{ij}\sqrt{G_r}\, e^{-j\Delta\varphi_{ij}}}{x_{ij} + x'_{ij}}\right|\right) + n \qquad i \in A_j \cup B_j \quad (66)$$

When d is relatively large, $x + x' \approx l \approx d$, $\theta \approx 0$, $G_l \approx G_r$, and $R \approx -1$, then (66) can be simplified into the following pathloss model

$$P_{ij} = P_{0j} + 10\log_{10}(G_r h_t^2 h_r^2) - 40\log_{10}\left(d_{ij}\right) + n \qquad i \in A_j \cup B_j \quad (67)$$

By rearranging the terms and dividing both sides by 20 and taking the power of 10 on both sides (67) can be written as follows

$$\Upsilon_{ij} \times h_{ij} = \alpha_{0j} \times 10^{\frac{n}{20}} \qquad i \in A_j \cup B_j \quad (68)$$

For sufficiently small noise, the right-hand side of (68) can be approximated using the first-order Taylor series expansion as

$$\Upsilon_{ij} \times h_{ij} = \alpha_{0j} + \epsilon_j \qquad i \in A_j \cup B_j \quad (69)$$

where $\Upsilon_{ij} = 10^{\frac{P_{ij}}{20}}$, $\alpha_{0j} = \sqrt{G_r} h_t h_r\, 10^{\frac{P_{0j}}{20}}$, $h_{ij} = d_{ij}^2$ and ϵ_j is the is a zero-mean Gaussian random variable with variance $\left(\frac{\alpha_{0j}\ln 10}{20}\sigma\right)^2$

$$d_{ij} = \sqrt{\left(x_j - a_i\right)^2 + \left(y_j - b_i\right)^2} \qquad i \in \mathrm{A}_j \quad (70)$$

$$d_{ij}^c = \sqrt{\left(x_j - y_i\right)^2 + \left(y_j - y_i\right)^2} \qquad i \in \mathrm{B}_j \quad (71)$$

Noncooperative Semidefinite Programing

$$\underset{[\boldsymbol{x},h_{ij},\alpha_{0\mathrm{j}}]}{\text{minimize}} \sum_{j\in\mathcal{L}} \sum_{i\in \mathrm{A}_j \cup \mathrm{B}_j} \left(\Upsilon_{ij} \times h_{ij} - \alpha_{0\mathrm{j}}\right)^2 \qquad i \in \mathrm{A}_j \quad (72)$$

subject to

$$h_{ij} = \boldsymbol{y}_i^T \boldsymbol{y}_i + \boldsymbol{x}_j^T \boldsymbol{x}_j - \mathbf{2}\boldsymbol{y}_i^T \boldsymbol{x}_j \qquad i \in \mathrm{A}_j \quad (73)$$

The objective function (72) is convex. However, the constraint (73) is not convex since the left-hand side is an affine expression and the right-hand side is a quadratic expression. By introducing an auxiliary variable $z_j = \boldsymbol{x}_j^T \boldsymbol{x}_j$ the constraint in the above equation can be written as follows

$$\underset{[\boldsymbol{x},h_{ij},z_i,\alpha_{0\mathrm{j}}]}{\text{minimize}} \sum_{j\in\mathcal{L}} \sum_{i\in \mathrm{A}_j \cup \mathrm{B}_j} \left(\Upsilon_{ij} \times h_{ij} - \alpha_{0\mathrm{j}}\right)^2 \qquad i \in \mathrm{A}_j \quad (74)$$

subject to

$$h_{ij} = \boldsymbol{y}_i^T \boldsymbol{y}_i + z_j - \mathbf{2}\boldsymbol{y}_i^T \boldsymbol{x}_j \qquad i \in \mathrm{A}_j \quad (75)$$

$$z_j = \boldsymbol{x}_j^T \boldsymbol{x}_j \quad (76)$$

the constraint (75) is convex now, however (76) is not since the left-hand side is an affine expression and the right-hand side is a quadratic. By relaxing the equality constraint (76) into inequality, the problem will be a convex optimization problem, which can be written as follows

$$\underset{[\boldsymbol{x},h_{ij},z_i,\alpha_{0\mathrm{j}}]}{\text{minimize}} \sum_{j\in\mathcal{L}} \sum_{i\in \mathrm{A}_j \cup \mathrm{B}_j} \left(\Upsilon_{ij} \times h_{ij} - \alpha_{0\mathrm{j}}\right)^2 \qquad i \in \mathrm{A}_j \quad (77)$$

subject to

$$h_{ij} = \boldsymbol{y}_i^T \boldsymbol{y}_i + z_j - \mathbf{2}\boldsymbol{y}_i^T \boldsymbol{x_j} \qquad i \in \mathrm{A}_j \qquad (78)$$

$$z_j \geq \boldsymbol{x}_j^T \boldsymbol{x}_j \qquad (79)$$

The constraints can be written equivalently as LMI as follows

$$\underset{[\boldsymbol{x}_j, z_j, h_{ij}, \alpha_{0\mathrm{j}}]}{\text{minimize}} \sum_{i \in \mathrm{A}_j} \left(\Upsilon_{ij} \times h_{ij} - \alpha_{0\mathrm{j}}\right)^2 \qquad i \in \mathrm{A}_j$$

subject to

$$h_{ij} = \begin{bmatrix} \boldsymbol{y}_i \\ -1 \end{bmatrix}^{\boldsymbol{T}} \begin{bmatrix} \boldsymbol{I_2} & \boldsymbol{x}_j \\ \boldsymbol{x}_j^T & z_j \end{bmatrix} \begin{bmatrix} \boldsymbol{y}_i \\ -1 \end{bmatrix} \qquad i \in \mathrm{A}_j$$

$$\begin{bmatrix} \boldsymbol{I_2} & \boldsymbol{x}_j \\ \boldsymbol{x}_j^T & z_j \end{bmatrix} \succcurlyeq \mathbf{0_3} \qquad i \in \mathrm{A}_j \quad (80)$$

Cooperative Semidefinite Programing

$$\underset{[\boldsymbol{x},h_{ij},\alpha_{0\mathrm{j}}]}{\text{minimize}} \sum_{j\in\mathcal{L}} \sum_{i\in \mathrm{A}_j \cup \mathrm{B}_j} \left(\Upsilon_{ij} \times h_{ij} - \alpha_{0\mathrm{j}}\right)^2 \qquad i \in \mathrm{A}_j \cup \mathrm{B}_j \quad (81)$$

subject to

$$h_{ij} = \boldsymbol{y}_i^T \boldsymbol{y}_i + z_j - \mathbf{2}\boldsymbol{y}_i^T \boldsymbol{x}_{\boldsymbol{j}} \qquad i \in \mathrm{A}_j \quad (82)$$

$$h_{ij} = \boldsymbol{x}_i^T \boldsymbol{x}_i + \boldsymbol{x}_{\boldsymbol{j}}^{\boldsymbol{T}} \boldsymbol{x}_{\boldsymbol{j}} - \mathbf{2}\boldsymbol{x}_i^T \boldsymbol{x}_{\boldsymbol{j}} \qquad i \in \mathrm{B}_j \quad (83)$$

The objective function (81) is convex. However, the constraints (82) and (83) are not convex since the the left-hand side is an affine expression and the right-hand side is a quadratic. By introducing an auxiliary variable $z_{ij} = \boldsymbol{x}_i^T \boldsymbol{x}_j$ the constraints in the above equation can be written as follows

$$\underset{[\boldsymbol{x},z_{ij},h_{ij},\alpha_{0\mathrm{j}}]}{\text{minimize}} \sum_{j\in\mathcal{L}} \sum_{i\in \mathrm{A}_j \cup \mathrm{B}_j} \left(\Upsilon_{ij} \times h_{ij} - \alpha_{0\mathrm{j}}\right)^2 \qquad i \in \mathrm{A}_j \cup \mathrm{B}_j \quad (84)$$

subject to

$$h_{ij} = \boldsymbol{y}_i^T \boldsymbol{y}_i + z_{jj} - \mathbf{2}\boldsymbol{y}_i^T \boldsymbol{x}_{\boldsymbol{j}} \qquad i \in \mathrm{A}_j \quad (85)$$

$$h_{ij} = z_{ii} + z_{jj} - 2z_{ij} \qquad i \in \mathrm{B}_j \quad (86)$$

$$z_{ij} = \boldsymbol{x}_i^T \boldsymbol{x}_j \qquad i \in \mathrm{A}_j \cup \mathrm{B}_j \quad (87)$$

the constraints (85) and (86) are convex now, however (87) is not since the left-hand side is an affine expression and the right-hand side is a quadratic. By relaxing the equality constraint (87) into inequality, the problem will be a convex optimization problem. Which can be written as follows

$$\underset{[\boldsymbol{x},z_{ij},h_{ij},\alpha_{0\mathrm{j}}]}{\text{minimize}} \sum_{j\in\mathcal{L}} \sum_{i\in \mathrm{A}_j \cup \mathrm{B}_j} \left(\Upsilon_{ij} \times h_{ij} - \alpha_{0\mathrm{j}}\right)^2 \qquad i \in \mathrm{A}_j \cup \mathrm{B}_j \quad (88)$$

subject to

$$h_{ij} = \boldsymbol{y}_i^T \boldsymbol{y}_i + z_{jj} - \mathbf{2}\boldsymbol{y}_i^T \boldsymbol{x_j} \qquad i \in \mathrm{A}_j \quad (89)$$

$$h_{ij} = z_{ii} + z_{jj} - 2z_{ij} \qquad i \in \mathrm{B}_j \quad (90)$$

$$z_{ij} \geq \boldsymbol{x}_i^T \boldsymbol{x}_j \qquad i \in \mathrm{A}_j \cup \mathrm{B}_j \quad (91)$$

The constraints can be written equivalently as LMI as follows

$$\underset{[\boldsymbol{x},\boldsymbol{z},h_{ij},\alpha_{0\mathrm{j}}]}{\text{minimize}} \sum_{j\in\mathcal{L}} \sum_{i\in \mathrm{A}_j \cup \mathrm{B}_j} \left(\Upsilon_{ij} \times h_{ij} - \alpha_{0\mathrm{j}}\right)^2 \qquad i \in \mathrm{A}_j \cup \mathrm{B}_j$$

subject to

$$h_{ij} = \begin{bmatrix} \boldsymbol{y}_i \\ -\mathbf{e}_j \end{bmatrix}^T \begin{bmatrix} \boldsymbol{I}_2 & \boldsymbol{x} \\ \boldsymbol{x}^T & \boldsymbol{z} \end{bmatrix} \begin{bmatrix} \boldsymbol{y}_i \\ -\mathbf{e}_j \end{bmatrix} \qquad i \in \mathrm{A}_j$$

$$h_{ij} = \begin{bmatrix} \mathbf{0}_2 \\ \mathbf{e}_i - \mathbf{e}_j \end{bmatrix}^T \begin{bmatrix} \boldsymbol{I}_2 & \boldsymbol{x} \\ \boldsymbol{x^T} & \boldsymbol{z} \end{bmatrix} \begin{bmatrix} \mathbf{0}_2 \\ \mathbf{e}_i - \mathbf{e}_j \end{bmatrix} \qquad i \in \mathrm{B}_j$$

$$\begin{bmatrix} \boldsymbol{I}_2 & \boldsymbol{x} \\ \boldsymbol{x}^T & \boldsymbol{z} \end{bmatrix} \succcurlyeq \mathbf{0}_{N+2} \quad (92)$$

where $\boldsymbol{z} = \boldsymbol{x}^T \boldsymbol{x}$ and $\mathbf{e}_j$ is a column vector with zero elements except the j^{th} element which equals 1.

References

[1] V. A. Reddy, G. L. Stüber, S. Al-Dharrab, A. H. Muqaibel, and W. Mesbah, "An energy-efficient IEEE 802.11ad mesh network for seismic acquisition," in *IEEE 91st Vehicular Technology Conference*, May 2020, pp. 1-5.

[2] C. Bagaini, T. Bunting, A. El-Emam, A. Laake, and C. Strobbia, "Land seismic techniques for high-quality data," *Oilf. Rev.*, vol. 22, no. 2, pp. 28–39, 2010.

[3] V. A. Reddy, G. L. Stüber, and S. Al-Dharrab, "High-speed seismic data acquisition over mm-wave channels," in *IEEE 88th Vehicular Technology Conference*, Jul. 2018, pp. 1-5.

[4] S. Savazzi, U. Spagnolini, L. Goratti, D. Molteni, M. Latva-Aho, and M. Nicoli, "Ultra-wide band sensor networks in oil and gas explorations," *IEEE Commun. Mag.*, vol. 51, no. 4, pp. 150–160, 2013.

[5] D. R. Santoso, S. Maryanto, A. Nadhir, and T. Sugiharto, "A simple and low-cost data acquisition system with multi-nodes facility for geophone array sensors," *Int. J. Appl. Eng. Res.*, vol. 12, no. 10, pp. 2109–2114, 2017.

[6] V. A. Reddy, G. L. Stüber, and S. Al-Dharrab, "Energy efficient network architecture for seismic data acquisition via wireless geophones," in *IEEE International Conference on Communications*, Jul. 2018, pp. 1-5.

[7] T. Ahmad, X. J. Li, B. C. Seet, and J. C. Cano, "Social network analysis based localization technique with clustered closeness centrality for 3D wireless sensor networks," *Electron.*, vol. 9, no. 5, 2020.

[8] S. Frattasi and F. Della Rosa, *Mobile Positioning and Tracking*, vol. 6, no. 49. Chichester, UK: John Wiley & Sons, Ltd, 2017.

[9] S. Savazzi and U. Spagnolini, "Wireless geophone networks for high-density land acquisition: Technologies and future potential," *Lead. Edge (Tulsa, OK)*, vol. 27, no. 7, pp. 882–886, 2008.

[10] L. Cheng, C. Wu, Y. Zhang, H. Wu, M. Li, and C. Maple, "A survey of localization in wireless sensor network," *Int. J. Distrib. Sens. Networks*, vol. 8, no. 12, 2012.

[11] A. Goldsmith, *Wireless communications*. Cambridge University Press, 2005.

[12] A. Larsson, A. Piotrowski, T. Giles, and D. Smart, "Near-earth RF propagation - Path loss and variation with weather," *2013 Int. Conf. Radar - Beyond Orthodox. New Paradig. Radar, RADAR 2013*, September 2013, pp. 57–63.

[13] M. Rodríguez, R. Feick, H. Carrasco, R. Valenzuela, M. Derpich, and L. Ahumada, "Wireless access channels with near-ground Level Antennas," *IEEE Trans. Wirel. Commun.*, vol. 11, no. 6, pp. 2204–2211, Jun. 2012.

[14] A. Torabi and S. A. Reza Zekavat, "Near-ground channel modeling with applications in wireless sensor networks and autonomous driving," in *Handbook of Position Location*, Wiley, 2019, pp. 1289–1308.

[15] G. G. Joshi et al., "Near-ground channel measurements over line-of-sight and forested paths," in *IEE Proceedings: Microwaves, Antennas and Propagation*, Dec. 2005, vol. 152, no. 6, pp. 589–596.

[16] M. Laaraiedh, L. Yu, S. Avrillon, and B. Uguen, "Comparison of hybrid localization schemes using RSSI, TOA, and TDOA," *17th Eur. Wirel. Conf. 2011, EW 2011*, 2011, pp. 626–630.

[17] U. Redlich, "Localization Techniques," *CT- MR-Guided Interv. Radiol.*, pp. 151–155, 2009.

[18] N. A. Azmi, S. Samsul, Y. Yamada, M. F. Mohd Yakub, M. I. Mohd Ismail, and R. A. Dziyauddin, "A Survey of localization using RSSI and TDoA techniques in wireless sensor network: System architecture," *2nd Int. Conf. Telemat. Futur. Gener. Networks, TAFGEN 2018*, pp. 131–136.

[19] R. Gong, J. Zhao, Y. Huang, and X. Meng, "WSN multilateral localization algorithm based on MLE," *Proc. - 2011 Int. Conf. Netw. Comput. Inf. Secur. NCIS 2011*, vol. 2, no. 1, pp. 426–429, 2011.

[20] M. Laaouafy, F. Lakrami, O. Labouidya, N. Elkamoun, and R. Iqdour, "Comparative study of localization methods in WSN using Cooja simulator," *7th Mediterr. Congr. Telecommun. 2019, C. 2019*, pp. 1–5.

[21] H. Khan, M. N. Hayat, and Z. Ur Rehman, "Wireless sensor networks free-range base localization schemes: A comprehensive survey," *Proc. 2017 Int. Conf. Commun. Comput. Digit. Syst. C-CODE 2017*, pp. 144–147.

[22] V. A. Reddy, A. Bazzi, G. L. Stüber, S. Al-Dharrab, W. Mesbah, and A. H. Muqaibel, "Fundamental performance limits of mm-wave cooperative localization in linear topologies," *IEEE Wirel. Commun. Lett.*, vol. 9, no. 11, pp. 1899–1903, 2020.

[23] A. Almehdhar et al., "DOA estimation in wireless seismic surveys using deep learning," *2020 Int. Conf. Commun. Signal Process. their Appl. (ICCSPA), Sharjah, United Arab Emirates, Accept.*, 2020.

[24] B. Bouhdid, W. Akkari, and A. Belghith, "Energy-aware cooperative localization approach for wireless sensor networks," *Proc. - 2017 IEEE 13th Int. Conf. Intell. Comput. Commun. Process. ICCP 2017*, pp. 429–435.

[25] M. Balaji and S. A. Chaudhry, "A cooperative trilateration technique for object localization," *Int. Conf. Adv. Commun. Technol. ICACT*, 2018, pp. 758–763.

[26] S. Tomic, M. Beko, R. Dinis, and L. Berbakov, "Cooperative localization in wireless sensor networks using combined measurements," *2015 23rd Telecommun. Forum, TELFOR 2015*, pp. 488–491.

[27] R. M. Vaghefi, M. R. Gholami, R. Michael Buehrer, and E. G. Strom, "Cooperative received signal strength-based sensor localization with unknown transmit powers," *IEEE Trans. Signal Process.*, vol. 61, no. 6, pp. 1389–1403.

[28] S. Tomic, M. Beko, and R. Dinis, "RSS-based localization in wireless sensor

networks using convex relaxation: Noncooperative and cooperative schemes," *IEEE Trans. Veh. Technol.*, vol. 64, no. 5, pp. 2037–2050.

[29] Y. Zou and H. Liu, "A Simple and efficient iterative method for Toa localization," *ICASSP, IEEE Int. Conf. Acoust. Speech Signal Process. - Proc.*, 2020, pp. 4881–4884.

[30] S. Wu, S. Zhang, and D. Huang, "A TOA-based localization algorithm with simultaneous NLOS mitigation and synchronization error elimination," *IEEE Sensors Lett.*, vol. 3, no. 3, 2019.

[31] H. Karl and A. Willig, *Protocols and Architectures for Wireless Sensor Networks*. Wiley, 2007.

[32] S. Bandaru and K. Deb, "Metaheuristic Techniques," *Decis. Sci. Theory Pract.*, pp. 693–749, 2016.

[33] Y. Wang, "Linear least squares localization in sensor networks," *Eurasip J. Wirel. Commun. Netw.*, vol. 2015, no. 1, pp. 1–7, 2015, doi: 10.1186/s13638-015-0298-1.

[34] S. M. Kay, *Fundamentals of Statistical Signal Processing: Estimation Theory*. Prentice Hall, 1997.

[35] R. W. Ouyang, A. K. S. Wong, C. T. Lea, and V. Y. Zhang, "Received signal strength-based wireless localization via semidefinite programming," *GLOBECOM - IEEE Glob. Telecommun. Conf.*, 2009, pp. 1307–1318.

[36] L. Vandenberghe and S. Boyd, "Semidefinite Programming," *SIAM Rev.*, vol. 38, no. 1, pp. 49–95, 1996, doi: 10.1137/1038003.

[37] R. Harikrishnan, V. J. S. Kumar, and P. Sridevi Ponmalar, "Differential evolution approach for localization in wireless sensor networks," 2014.

[38] E.-G. Talbi, *Metaheuristics : from design to implementation*. Hoboken, N.J. : John Wiley & Sons, 2009.

[39] O. J. Pandey, A. Mahajan, and R. M. Hegde, "Cooperative localization in small world wireless sensor networks," *2017 9th Int. Conf. Commun. Syst. Networks, COMSNETS 2017*, 2017, pp. 391–392.

[40] N. Patwari, J. N. Ash, S. Kyperountas, A. O. Hero, R. L. Moses, and N. S. Correal, "Locating the nodes: Cooperative localization in wireless sensor networks," *IEEE Signal Process. Mag.*, vol. 22, no. 4, pp. 54–69, 2005.

[41] S. Wang, F. Luo, and L. Zhang, "Universal cooperative localizer for WSN with varied types of ranging measurements," *IEEE Signal Process. Lett.*, vol. 24, no. 8, pp. 1223–1227, 2017.

[42] L. Zhang, Z. Wang, Z. Kuang, and H. Yang, "Three-dimensional localization algorithm for WSN nodes based on RSSI-TOA and LSSVR method," *Proc. - 2019 11th Int. Conf. Meas. Technol. Mechatronics Autom. ICMTMA 2019*, pp. 498–503.

[43] I. Güvenç and C. C. Chong, "A survey on TOA based wireless localization and NLOS mitigation techniques," *IEEE Commun. Surv. Tutorials*, vol. 11, no. 3, pp. 107–124, 2009.

[44] S. Chen and K. C. Ho, “Performance of square-range least squares and square-range least absolute deviations for the self-localization of sensor nodes using convex relaxations,” *Int. Conf. Digit. Signal Process. DSP*, 2019.

[45] C. Meng, Z. Ding, and S. Dasgupta, “A semidefinite programming approach to source localization in wireless sensor networks,” *IEEE Signal Process. Lett.*, vol. 15, pp. 253–256, 2008.

[46] Y. Nesterov, H. Wolkowicz, and Y. Ye, “Semidefinite programming relaxations of nonconvex quadratic optimization,” pp. 361–419, 2000.

[47] P. Biswas, T. C. Lian, T. C. Wang, and Y. Ye, “Semidefinite programming based algorithms for sensor network localization,” *ACM Trans. Sens. Networks*, vol. 2, no. 2, pp. 188–220, 2006.

[48] S. Ravindra and S. N. Jagadeesha, “Time of arrival based localization in wireless sensor networks: A linear approach,” *Signal Image Process. An Int. J.*, vol. 4, no. 4, pp. 13–30, 2013.

[49] R. M. Vaghefi and R. M. Buehrer, “Cooperative sensor localization with NLOS mitigation using semidefinite programming,” *WPNC’12 - Proc. 9th Work. Positioning, Navig. Commun.*, 2012, pp. 13–18.

[50] R. M. Vaghefi, J. Schloemann, and R. M. Buehrer, “NLOS mitigation in TOA-based localization using semidefinite programming,” *2013 10th Work. Positioning, Navig. Commun.*, 2013.

[51] R. M. Vaghefi and R. M. Buehrer, “Cooperative localization in NLOS environments using semidefinite programming,” *IEEE Commun. Lett.*, vol. 19, no. 8, pp. 1382–1385, 2015.

[52] M. Laaraiedh, S. Avrillon, and B. Uguen, “A maximum likelihood TOA based estimator for localization in heterogeneous networks,” *Int. J. Commun. Netw. Syst. Sci.*, vol. 03, no. 01, pp. 38–42, 2010.

Vitae

Name	:Mansour Aljarbue
Nationality	:Saudi
Date of Birth	:4/8/1993
Email	:maljarbue@gmail.com
Address	:152 Alqamar st, Riyadh , Saudi Arabia
Academic Background	:Electrical and Telecommunications Engineering

---

Education	:B.S Electrical Engineering, King Fahd University of Petroleum and Minerals, 2016
Career History	: (2016-2017) Wireless Solution Engineer at Huawei Tech : (2017-Current) Telecom Engineer at Saudi Aramco
Technical Certifications	: (2020) Certified Wireless Solutions Administrator : (2018) Cisco Certified Network Professional (CCNP) : (2018) Cisco Certified Network Associate (CCNA) : (2018) Juniper Enterprise Associate : (2018) Juniper Security Associate
Projects	:(2020-2021) Commissioning Video-Conferencing Solutions for Saudi Aramco Executives :(2020) Designing and commissioning the first LoRaWAN IoT solution in Saudi Aramco :(2019) New IT Infrastructure for Saudi Aramco logistics services :(2018) Network security compliance automation :(2018) Saudi Aramco Network optimization

References:

Dr. Suhail Ibrahim Al-Dharrab (Thesis Advisor)
Email: suhaild@kfupm.edu.sa
Phone: +966 13 860 8210

Ali Alshehri (Supervisor)
Email: Ali.Shehri.14@Aramco.com
Phone:+966 13 880 0233